NASA TECHNICAL NOTE

NASA TN D-4611

C. 1

NASA TN D-4611

STATIC-TEMPERATURE DISTRIBUTION IN A FLAT-PLATE COMPRESSIBLE TURBULENT BOUNDARY LAYER WITH HEAT TRANSFER

by S. Z. Pinckney

Langley Research Center
Langley Station, Hampton, Va.

NATIONAL AERONAUTICS AND SPACE ADMINISTRATION • WASHINGTON, D. C. • JUNE 1968

STATIC-TEMPERATURE DISTRIBUTION IN A FLAT-PLATE COMPRESSIBLE TURBULENT BOUNDARY LAYER WITH HEAT TRANSFER

By S. Z. Pinckney

Langley Research Center
Langley Station, Hampton, Va.

NATIONAL AERONAUTICS AND SPACE ADMINISTRATION

For sale by the Clearinghouse for Federal Scientific and Technical Information
Springfield, Virginia 22151 – CFSTI price $3.00

STATIC-TEMPERATURE DISTRIBUTION IN A FLAT-PLATE COMPRESSIBLE TURBULENT BOUNDARY LAYER WITH HEAT TRANSFER

By S. Z. Pinckney
Langley Research Center

SUMMARY

An expression based on the differential equations for the local energy transfer and shear is derived for the relationship between the static temperature and the velocity in a zero-pressure-gradient turbulent boundary layer. The boundary conditions imposed by these governing equations showed the temperature-velocity relation to be at least a fourth degree polynomial which differs considerably from the second degree polynomial obtained by previous investigators. These governing equations are integrated by using as boundary conditions the value of a particular total-energy-deficiency parameter of the boundary layer at the station under consideration, the slope of the laminar-sublayer temperature-velocity profile at the wall (as determined from a modified Reynolds analogy), and the local free-stream and wall conditions. Results obtained by this method are compared with experimental temperature-velocity profile data and are found to correlate well with the experimental profiles.

INTRODUCTION

The ability to predict the variation of turbulent-boundary-layer parameters, such as momentum, displacement, and energy thicknesses, is very important in supersonic flow. In order to describe the distribution of these parameters, a knowledge of the turbulent-boundary-layer temperature profile is needed, in addition to the velocity profile and friction coefficients.

The difficulties encountered in the theoretical evaluation, even for the zero-pressure-gradient turbulent boundary layer, have resulted in the extensive use of empirical correlations. For example, correlations for the compressible friction coefficient (ref. 1) and zero-pressure-gradient incompressible velocity profiles (ref. 2) have resulted in various empirical methods for the determination of these parameters.

Up to the present time, the temperature profile for the compressible turbulent boundary layer with heat transfer has not been correlated accurately even for zero

pressure gradient. The determination of temperature profiles has been limited, generally to attempts at altering an expression obtained by Luigi Crocco for laminar flow (this expression is presented in ref. 3). In reference 4, however, an expression for the temperature profile that is based on the differential equations for local energy transfer and shear is presented.

In the determination of the expression for the turbulent-boundary-layer temperature profile, it was assumed in reference 4 that the ratio of local energy transfer to wall heat transfer divided by the ratio of local shear to wall shear is a constant. Also the ratio of eddy diffusivity of heat to eddy diffusivity of momentum was assumed to be a constant across the boundary layer. It is pointed out in reference 4 that for flow over a flat plate this ratio of eddy diffusivities is approximately unity; therefore, most of the calculated results presented in reference 4 were derived with a value of 1 assumed for the ratio. In the present paper, a comparison of the results obtained by using the theoretical expression for the temperature profile of reference 4 with experimental data (ref. 5) reveals substantial differences between the theory and some flat-plate temperature profiles. This observed discrepancy between theory and experiment is believed to be due in part to the aforementioned assumptions, as well as to other simplifying assumptions. The method developed in the present paper avoids the difficulties of evaluating local values of some of the less tractable boundary-layer parameters by making use of an integral parameter which exerts a strong influence on the temperature profile.

The present analysis is similar in approach to that presented in reference 4, but a polynomial expression in terms of the ratio of local velocity to free-stream velocity is assumed for the ratio of local energy transfer to local shear, and a function which contains eddy diffusivities of heat and momentum as parameters is determined from certain boundary conditions. In particular, a boundary condition is imposed that requires the value of a particular total-energy-deficiency parameter of the boundary layer, determined from the theoretical static-temperature—velocity profile relation, be equal to the known value of the total-energy-deficiency parameter of the boundary layer at the station under consideration. The use of a total-energy-deficiency parameter is a new and reasonable approach to the problem based on the observation of many researchers that most turbulent-boundary-layer parameters are functions of the previous history of the boundary layer. At the present time, for example, in a design problem the lengthwise distribution of the total energy deficiency and the momentum thickness needed to determine the value of the total-energy-deficiency parameter could be determined by integration of the heat transfer to the wall and of momentum losses due to shear along the wall, respectively. In a converse sense, if the total energy deficiency and momentum thickness cannot be determined at a given station, the comparisons of experimental data and results from theories presented herein strongly imply that within the current state-of-the-art

the static-temperature—velocity profile cannot be determined with accuracy except for certain cases.

SYMBOLS

a	expression for $\dfrac{\frac{k}{c_p} + \rho\epsilon_h}{\mu + \rho\epsilon}$
b,c,d,e	constants assumed in the relationship between q/τ and u/u_∞
c_f	friction coefficient, $\dfrac{2\tau_w}{\rho_\infty u_\infty^2}$
c_p	specific heat of a fluid at constant pressure
h	static enthalpy $\left(\text{for perfect gas, } h = c_p T\right)$
k	thermal conductivity
M_∞	free-stream Mach number
N	exponent for y/δ in velocity profile relation $\left(\dfrac{u}{u_\infty} = \left(\dfrac{y}{\delta}\right)^{1/N}\right)$
Pr	Prandtl number, $\dfrac{c_p \mu}{k}$
q	energy transfer in y-direction, per unit time per unit area (as defined by eq. (2))
Q	total energy deficiency of boundary layer relative to free stream, $Q = \int_0^\delta \rho u\left(h_{t,\infty} - h_t\right) dy$
R	perfect gas constant
T	static temperature
T_t	total temperature
T_w^*	hypothetical wall temperature
u	velocity component parallel to plate

x	longitudinal distance along plate
y	perpendicular distance from plate
γ	ratio of specific heats, taken as 1.4 for air
δ	boundary-layer thickness
ϵ	eddy diffusivity of momentum
ϵ_h	eddy diffusivity of heat
θ	momentum thickness, $\int_0^\delta \frac{\rho u}{\rho_\infty u_\infty}\left(1 - \frac{u}{u_\infty}\right)dy$
μ	viscosity
ρ	density
τ	shear stress, force per unit area

Subscripts:

aw	adiabatic wall conditions
t	total conditions
w	wall conditions
∞	local free-stream conditions

ANALYSIS

Classically, the turbulent boundary layer is divided into three regions:

(1) The inner region or laminar sublayer;

(2) The transition region between the laminar sublayer and the turbulent flow region; and

(3) The turbulent flow region.

In deriving an expression for the turbulent-boundary-layer enthalpy-velocity distribution it was not necessary to distinguish between these three regions of the boundary layer. However, various features of two of these regions, namely the laminar sublayer and the turbulent flow region, are in evidence through the boundary conditions and the form of the equations for shear stress and energy transfer that are assumed.

From reference 4 the local shear and energy transfer in the boundary layer can be expressed as follows:

$$\tau = (\mu + \rho\epsilon)\frac{du}{dy} \tag{1}$$

$$q = -\left(\frac{k}{c_p} + \rho\epsilon_h\right)\frac{dh}{dy} - (\mu + \rho\epsilon)u\frac{du}{dy} \tag{2}$$

Dividing equation (2) by equation (1) and nondimensionalizing h and u with respect to the free stream give

$$\frac{q}{\tau} = -\frac{h_\infty}{u_\infty}\frac{\frac{k}{c_p} + \rho\epsilon_h}{\mu + \rho\epsilon}\frac{d\left(\frac{h}{h_\infty}\right)}{d\left(\frac{u}{u_\infty}\right)} - u_\infty\frac{u}{u_\infty} \tag{3}$$

In order to integrate equation (3) a knowledge of the relationships between q/τ and u and between $\frac{\frac{k}{c_p} + \rho\epsilon_h}{\mu + \rho\epsilon}$ and h is needed. Herein the ratio $\frac{\frac{k}{c_p} + \rho\epsilon_h}{\mu + \rho\epsilon}$ is assumed to be constant and is designated a.

The following third degree polynomial in terms of u/u_∞ is assumed for the relationship between the ratio q/τ and the velocity profile:

$$\frac{q}{\tau} = b + d\left(\frac{u}{u_\infty}\right) + e\left(\frac{u}{u_\infty}\right)^2 + c\left(\frac{u}{u_\infty}\right)^3 \tag{4}$$

From a consideration of the boundary conditions imposed on the governing equations (which are presented in appendix A of ref. 4) when a constant wall temperature is assumed,

$$\left(\frac{\partial\tau}{\partial y}\right)_w = \left(\frac{\partial q}{\partial y}\right)_w = 0 \tag{5a}$$

and

$$\left(\frac{\partial^2\tau}{\partial y^2}\right)_w = \left(\frac{\partial^2 q}{\partial y^2}\right)_w = 0 \tag{5b}$$

Applying the boundary conditions of equations (5a) and (5b) to equation (4) gives $d = 0$ and $e = 0$. Therefore, the polynomial assumed for the relationship between q/τ and the velocity profile reduces to

$$\frac{q}{\tau} = b + c\left(\frac{u}{u_\infty}\right)^3 \tag{6}$$

When a is substituted for $\frac{\frac{k}{c_p} + \rho\epsilon_h}{\mu + \rho\epsilon}$ and the expression for q/τ from equation (6) is used in equation (3), integration from the wall to an arbitrary point in the boundary layer gives, after rearranging,

$$\frac{h}{h_\infty} = \frac{h_w}{h_\infty} - \frac{u_\infty^2}{h_\infty}\left[\frac{b}{au_\infty}\frac{u}{u_\infty} + \frac{1}{2a}\left(\frac{u}{u_\infty}\right)^2 + \frac{c}{4au_\infty}\left(\frac{u}{u_\infty}\right)^4\right] \tag{7}$$

The coefficients a, b, and c in equation (7) are constant at a given station but vary with x; the evaluation of the constants is accomplished by using the following boundary conditions:

(1) From Colburn's version of Reynolds analogy,

$$\left[\frac{d\left(\frac{h}{h_\infty}\right)}{d\left(\frac{u}{u_\infty}\right)}\right]_w = \frac{h_{aw} - h_w}{h_\infty} Pr^{1/3}$$

(2) At the outer edge of the boundary layer, $\frac{h}{h_\infty} = 1.0$ and $\frac{u}{u_\infty} = 1.0$; and

(3) The integral of the total energy deficiency across the boundary layer evaluated by combining the enthalpy relation derived from equation (7) with a suitable assumed velocity profile must equal the total enthalpy deficiency of the entire boundary layer up to the x-station under consideration. A derivation for the total-energy-deficiency parameter is presented in appendix A.

The differentiation of equation (7) and the evaluation of the result at the wall give

$$\left[\frac{d\left(\frac{h}{h_\infty}\right)}{d\left(\frac{u}{u_\infty}\right)}\right]_w = -\frac{u_\infty}{h_\infty}\frac{b}{a} \tag{8}$$

The application of boundary condition (2) to equation (7) and the substitution of equation (8) into the result give

$$\frac{u_\infty^2}{2ah_\infty} = -1 + \left[\frac{d\left(\frac{h}{h_\infty}\right)}{d\left(\frac{u}{u_\infty}\right)}\right]_w + \frac{h_w}{h_\infty} - \frac{u_\infty}{4h_\infty}\frac{c}{a} \tag{9}$$

The substitution of equations (8) and (9) into equation (7) leads to

$$\frac{h}{h_\infty} = \frac{h_w}{h_\infty} + \left[\frac{d\left(\frac{h}{h_\infty}\right)}{d\left(\frac{u}{u_\infty}\right)}\right]_w \frac{u}{u_\infty} + \left\{1 - \left[\frac{d\left(\frac{h}{h_\infty}\right)}{d\left(\frac{u}{u_\infty}\right)}\right]_w - \frac{h_w}{h_\infty} + \frac{u_\infty}{4h_\infty}\frac{c}{a}\right\}\left(\frac{u}{u_\infty}\right)^2 - \frac{u_\infty}{4h_\infty}\frac{c}{a}\left(\frac{u}{u_\infty}\right)^4 \tag{10}$$

and the rearrangement of equation (10) using boundary condition (1) gives

$$\frac{h}{h_\infty} = \frac{h_w}{h_\infty} + \left(1 - \frac{h_w}{h_\infty}\right)\left(\frac{u}{u_\infty}\right)^2 + \left[\frac{u}{u_\infty} - \left(\frac{u}{u_\infty}\right)^2\right]\frac{h_{aw} - h_w}{h_\infty}\,Pr^{1/3} + \frac{u_\infty}{4h_\infty}\frac{c}{a}\left[\left(\frac{u}{u_\infty}\right)^2 - \left(\frac{u}{u_\infty}\right)^4\right] \tag{11}$$

With the assumption of a perfect gas $\left(\text{for which } h = c_p T\right)$, equation (11) can be rearranged to give

$$\frac{T}{T_\infty} = \frac{T_w}{T_\infty} + \left(1 - \frac{T_w}{T_\infty}\right)\left(\frac{u}{u_\infty}\right)^2 + \left[\frac{u}{u_\infty} - \left(\frac{u}{u_\infty}\right)^2\right]\frac{T_{aw} - T_w}{T_\infty}\,Pr^{1/3} + \frac{(\gamma - 1)M_\infty^2}{4u_\infty}\frac{c}{a}\left[\left(\frac{u}{u_\infty}\right)^2 - \left(\frac{u}{u_\infty}\right)^4\right] \tag{12}$$

In equations (11) and (12) the only remaining unknown is the ratio of constants c/a. The final form of equation (11) or (12) and the value for the ratio c/a are determined through application of boundary condition (3). This boundary condition requires the matching of the value of the total-energy-deficiency parameter determined by using equation (A3) in conjunction with the theoretical enthalpy-velocity or temperature-velocity profile relation (eq. (11) or (12), respectively) with the known value of the total-energy-deficiency parameter of the boundary layer at the station under consideration. This matching process and thus the determination of the correct value for the ratio of constants c/a consist of the substitution of the theoretical enthalpy-velocity or temperature-velocity profile relation along with a suitable velocity profile into the right-hand side of equation (A3) and iterating, with several values tried for the unknown c/a. This iteration is complete and the correct value for the ratio of constants c/a is determined when the right-hand side of equation (A3) produces a value for the total-energy-deficiency parameter equal to the known value. In practical application of the present theoretical method, the total energy deficiency and the momentum thickness needed to determine the known value of the total-energy-deficiency parameter would be determined from the heat loss to the wall and friction losses along the wall integrated from the boundary-layer origin to the x-station under consideration. However, in the present comparisons of experimental data and theoretical results, sufficient information for performing this type of integration accurately generally was not available; therefore data were chosen for which the total temperatures across the boundary layer were

available (see table I) and the known value of the total-energy-deficiency parameter could be determined from the experimental profiles.

RESULTS AND DISCUSSION

Comparisons of Theory and Experiment

The present theoretical results have been compared with 82 experimental temperature-velocity profiles obtained from references 5 to 14. The results of these comparisons are presented in figures 1 to 9. For these comparisons a power-law velocity profile of the form $\frac{u}{u_\infty} = \left(\frac{y}{\delta}\right)^{1/N}$ was assumed. Theoretical temperature-velocity profiles were obtained for comparison with each experimental temperature-velocity profile by using a high-speed digital-computer program, with values of 5, 7, and 9 assumed for the power-law velocity-profile exponent N. As exemplified by figures 1(a) and 1(b), the theoretical temperature-velocity profile is a weak function of the power-law velocity profile assumed. As a result it was considered sufficient to present in figures 2 to 9 only the theoretical curves corresponding to a power-law exponent of 5, with the exception of figure 8(d). Because the experimental velocity profile for the experimental data of figure 8(d) corresponded to an N value of approximately 20, the theoretical temperature-velocity profile of figure 8(d) was also determined with $\frac{u}{u_\infty} = \left(\frac{y}{\delta}\right)^{1/20}$ as the assumed velocity profile relation. It is evident that the 1/5-power profile is not as adequate an approximation for these experimental data as it was for the other experimental data presented.

For comparison purposes figures 1(a) and 1(b) include sample theoretical temperature-velocity profiles calculated by using the theoretical method of reference 4 as well as sample profiles calculated by using the modified Crocco distribution assumed in reference 15. Figure 10 shows sample experimental velocity profiles which correspond to some of the experimental temperature-velocity profiles; also shown in figure 10 for comparison purposes is a 1/7-power velocity profile.

The experimental temperature-velocity profiles considered in this presentation are for a range of M_∞ from 0.85 to 8.18 and a range of T_w/T_∞ from 0.997 to 7.38. In general, comparisons between results of the present theory and experimental data showed maximum discrepancies between point values of temperature of approximately 5 percent for the outer 90 percent of the boundary layer (values of y/δ between 0.1 and 1.0) and approximately 10 percent for the inner 10 percent of the boundary layer (values of y/δ less than 0.1). In comparisons involving the data of reference 8 (fig. 4) the discrepancies are larger, approximately 19 percent at distances from the wall of 0.3 millimeter – that is, for $y/\delta = 0.05$. The discrepancies are within 10 percent at values of velocity ratio

greater than 0.75 or at distances from the wall greater than 0.5 millimeter – that is, for $y/\delta > 0.08$. The reason for the larger discrepancies between the results of the present theory and the data from this reference is not known; however, it was indicated in references 16 and 17 that the experimental values of c_f in reference 8 are considered unreliable. Reference 17 also indicated that the profile data of reference 8 may have been taken in a transition region. In particular, it should be noted that the experimental temperature-velocity data of reference 8 seem to show inconsistencies between profiles. For example, the experimental temperature-velocity profiles of figures 4(m) and 4(n) have essentially the same boundary conditions:

Figure	M_∞	u_∞, meters/second	Reynolds number based on θ	Stagnation pressure, atm*	T_w/T_∞
4(m)	5.26	791.0	3880	7.31	5.463
4(n)	5.29	786.6	4300	7.09	5.564

*1 atmosphere = 101 325 N/m^2.

However, a comparison of the experimental total-energy-deficiency profiles corresponding to the data in figures 4(m) and 4(n), as presented in figure 11, shows significant differences, with the more downstream profile (that corresponding to the data in fig. 4(n)) having the lower total energy deficiency.

In the present comparison of theoretical results and experimental data, the apparent absence of any effect resulting from not considering the laminar-sublayer velocity profile is believed to be due to the existence of thin laminar sublayers. The thickness of the laminar sublayers of the experimental data corresponds approximately to only 5 to 10 percent of the total boundary-layer thickness and therefore makes little difference to any integral across the boundary layer. As a matter of interest, the edge of the laminar sublayer as estimated by the relation $\frac{u}{u_\infty} = 12\sqrt{\frac{T_w}{T_\infty}\frac{c_f}{2}}$ (ref. 2) is presented in figure 1. It is believed that the use of an assumed power-law velocity profile in the theoretical calculations must be restricted to turbulent boundary layers with relatively thin laminar sublayers.

Index Parameter for Ideal Flat-Plate Flow

As discussed in the introduction, most previous attempts to express the relationship for the turbulent-boundary-layer temperature-velocity profile have been restricted to modifications of the expression obtained by Crocco for laminar flow. A typical example of these temperature-velocity profile relationships (ref. 15) is

$$\frac{T}{T_\infty} = 1 + \frac{\gamma - 1}{2} Pr^{1/3} M_\infty^2 \left[1 - \left(\frac{u}{u_\infty}\right)^2\right] + \frac{T_w - T_{aw}}{T_\infty}\left(1 - \frac{u}{u_\infty}\right) \tag{13}$$

For certain examples (see fig. 1(b)), experimental data were found to correspond closely to results from equation (13) (method of ref. 15) as well as to results obtained by the theoretical method of reference 4. In other examples (see fig. 1(a)), significant differences between experimental data and results obtained by using the methods of references 4 and 15 are evident. It should be noted that the difference in theory and experiment shown in figure 1(a) could result in as much as a 50-percent error in a computation of boundary-layer displacement thickness. Therefore the theoretical methods of references 4 and 15 were explored further by examining the derivation of the pertinent governing equations. This examination revealed that the theoretical derivations had as a basis the assumption of the existence of a constant flat-plate surface temperature and free-stream Mach number from the plate leading edge to the station under consideration. Based on these assumptions, Colburn's form of Reynolds analogy gives (for a perfect gas) the total energy deficiency at the station under consideration as

$$Q = \frac{\rho_\infty u_\infty c_p T_\infty}{Pr^{2/3}}\left(\frac{T_{aw} - T_w}{T_\infty}\right)\theta \tag{14}$$

or, solved for T_w/T_∞,

$$\frac{T_w}{T_\infty} = \frac{T_{aw}}{T_\infty} - \frac{Pr^{2/3} Q}{T_\infty \rho_\infty u_\infty c_{p,\infty} \theta} \tag{15}$$

On the basis of these observations for flat-plate flow, it is believed that good correspondence between experimental data and the theoretical results of references 4 and 15 can be obtained when T_w/T_∞, Q, and θ are related as indicated by equation (15), which corresponds to ideal flat-plate flow.

From this discussion, it is apparent that an index parameter is needed to provide a quantitative value for the deviation of a profile from ideal flat-plate flow. Equation (15) may be used for this purpose. For ideal flat-plate flow to exist, the wall-temperature ratio T_w/T_∞ must equal the difference between the adiabatic-wall-temperature ratio T_{aw}/T_∞ and the total-energy-deficiency parameter $\frac{Pr^{2/3} Q}{T_\infty \rho_\infty u_\infty c_{p,\infty} \theta}$ (see eq. (15)). The total-energy-deficiency parameter $\frac{Pr^{2/3} Q}{T_\infty \rho_\infty u_\infty c_{p,\infty} \theta}$ is directly proportional to the total-energy-deficiency parameter $\frac{Q}{\rho_\infty u_\infty h_{t,\infty} \theta}$ used in this report as a boundary condition to determine the ratio of constants c/a of equation (11) or (12). When the boundary layer

does not correspond to ideal flat-plate flow, the wall temperature T_w of equation (15) is arbitrarily replaced by the hypothetical wall temperature T_w^* and thus the following equation is generated:

$$\frac{T_w^*}{T_\infty} = \frac{T_{aw}}{T_\infty} - \frac{Pr^{2/3}Q}{T_\infty \rho_\infty u_\infty c_{p,\infty} \theta} \tag{16}$$

Now T_w^* is defined as the hypothetical wall temperature required under ideal flat-plate flow conditions to produce a given value of the total-energy-deficiency parameter. Thus the difference between T_w and T_w^* is a measure of the deviation from ideal flat-plate flow as well as a function of the total-energy-deficiency parameter. The value of $\frac{T_w - T_w^*}{T_w^*}$ along with other pertinent information is presented in table I for each experimental temperature-velocity profile considered. Since the index parameter $\frac{T_w - T_w^*}{T_w^*}$ and the ratio of constants c/a are both functions of the total-energy-deficiency parameter $\frac{Q}{\rho_\infty u_\infty h_{t,\infty} \theta}$, a means is suggested for the correlation of the ratio of constants c/a needed for use in the present theoretical enthalpy-velocity or temperature-velocity relation of equation (11) or (12). Equation (16) was combined with the perfect-gas version of the theoretical temperature-velocity relation (eq. (12)) with the use of a high-speed digital-computer program, and the set of curves presented in figure 12 were generated. The curves in figure 12 are for a power-law exponent of 7 and free-stream Mach numbers of 3, 5, and 7. Each curve is for a particular ratio of wall to free-stream temperature. Figure 12 can be used to determine a value for the ratio of constants c/a directly, instead of by iteration. For example, the integrated total energy deficiency Q and the momentum thickness θ needed for use in equation (16) would be determined from the heat loss to the wall and friction losses along the wall integrated from the boundary-layer origin to the x-station under consideration. Then use of these values of Q and θ in equation (16) would produce a value of T_w^*. Upon combining the resulting value of T_w^* with the wall temperature T_w, the value of $\frac{T_w - T_w^*}{T_w^*}$ needed for entrance into figure 12 would be obtained. The resulting value of c/a would be the same as that which would be obtained by the iteration process with a 1/7-power velocity profile used in the energy-deficiency integral of equation (A3).

CONCLUDING REMARKS

The present method for computing the static-temperature—velocity distribution for a zero-pressure-gradient compressible turbulent boundary layer has been developed by using as a boundary condition the known value of a particular total-energy-deficiency

parameter of the boundary layer at the station under consideration. In comparing results of this analytical method with experimental data, a power-law turbulent-boundary-layer velocity profile was assumed. It was observed that the analytical results are a weak function of the power-law velocity profile assumed and that the theory produces results which agree well with the experimental data. The experimental velocity profiles, for which the power-law assumption gives good correspondence, are restricted to turbulent boundary layers that have thin laminar sublayers. For boundary layers with relatively thick laminar sublayers, more accurate velocity profile representations should be used.

A comparison of experimental temperature-velocity profiles with modified Crocco flat-plate turbulent-boundary-layer temperature-velocity relations revealed that correlation with experimental profiles is obtained when the experimental data correspond to ideal flat-plate flow. The present method gives good agreement for all experimental profiles examined, including those for ideal flat-plate flow and those for gross deviations from ideal flat-plate flow.

Langley Research Center,
National Aeronautics and Space Administration,
Langley Station, Hampton, Va., February 28, 1968,
126-15-03-01-23.

APPENDIX A

EQUATION FOR TOTAL ENERGY DEFICIENCY

The total energy transferred to the wall upstream of a particular boundary-layer station can be obtained by the integration of the energy deficiency of the boundary layer relative to the free stream. The result is

$$Q = \int_0^{\delta} \rho u h_{t,\infty}\, dy - \int_0^{\delta} \rho u h_t\, dy \tag{A1}$$

which is equivalent to $Q = \int_0^x q_w\, dx$. After rearranging, equation (A1) becomes

$$\frac{Q}{\rho_\infty u_\infty h_{t,\infty}\delta} = \int_0^1 \frac{u}{u_\infty}\frac{T_\infty}{T}\left[1 - \frac{h}{h_{t,\infty}} - \frac{\gamma - 1}{2} M_\infty^2 \frac{h_\infty}{h_{t,\infty}}\left(\frac{u}{u_\infty}\right)^2\right] d\left(\frac{y}{\delta}\right) \tag{A2}$$

or, after dividing by θ/δ,

$$\frac{Q}{\rho_\infty u_\infty h_{t,\infty}\theta} = \frac{\int_0^1 \frac{u}{u_\infty}\frac{T_\infty}{T}\left[1 - \frac{h}{h_{t,\infty}} - \frac{\gamma - 1}{2} M_\infty^2 \frac{h_\infty}{h_{t,\infty}}\left(\frac{u}{u_\infty}\right)^2\right] d\left(\frac{y}{\delta}\right)}{\int_0^1 \frac{T_\infty}{T}\frac{u}{u_\infty}\left(1 - \frac{u}{u_\infty}\right) d\left(\frac{y}{\delta}\right)} \tag{A3}$$

REFERENCES

1. Nestler, D. E.; and Goetz, R.: Survey of Theoretical and Experimental Determinations of Skin Friction in Compressible Boundary Layers: Part II. The Turbulent Boundary on a Flat Plate. Tech. Inform. Ser. No. R58SD270 (Contract AF 04(645)-24), Missile Ord. Syst. Dep., Gen. Elec. Co., Jan. 29, 1959.

2. Cornish, Joseph Jenkins, III: A Universal Description of Turbulent Boundary Layer Profiles With or Without Transpiration. Res. Rep. No. 29 (Contract NONR 978(01)), Aerophys. Dep., Mississippi State Univ., June 1, 1960.

3. Van Driest, E. R.: Investigation of Laminar Boundary Layer in Compressible Fluids Using the Crocco Method. NACA TN 2597, 1952.

4. Deissler, R. G.; and Loeffler, A. L., Jr.: Analysis of Turbulent Flow and Heat Transfer on a Flat Plate at High Mach Numbers With Variable Fluid Properties. NASA TR R-17, 1959. (Supersedes NACA TN 4262.)

5. Lobb, R. Kenneth; Winkler, Eva M.; and Persh, Jerome: Experimental Investigation of Turbulent Boundary Layers in Hypersonic Flow. J. Aeronaut. Sci., vol. 22, no. 1, Jan. 1955, pp. 1-9, 50.

6. Kepler, C. E.; and O'Brien, R. L.: Supersonic Turbulent Boundary Layer Growth Over Cooled Walls in Adverse Pressure Gradients. ASD-TDR-62-87, U.S. Air Force, Oct. 1962.

7. Lobb, R. Kenneth; Winkler, Eva M.; and Persh, Jerome: NOL Hypersonic Tunnel No. 4 Results VII: Experimental Investigation of Turbulent Boundary Layers in Hypersonic Flow. NAVORD Rep. 3880, U.S. Nav. Ord. Lab., Mar. 1, 1955.

8. Winkler, Eva M.; and Cha, Moon H.: Investigation of Flat Plate Hypersonic Turbulent Boundary Layers With Heat Transfer at a Mach Number of 5.2. NAVORD Rep. 6631, U.S. Nav. Ord. Lab., Sept. 15, 1959.

9. Pinckney, S. Z.: Data on Effects of Incident-Reflecting Shocks on the Turbulent Boundary Layer. NASA TM X-1221, 1966.

10. Nothwang, George J.: An Evaluation of Four Experimental Methods for Measuring Mean Properties of a Supersonic Turbulent Boundary Layer. NACA Rep. 1320, 1957. (Supersedes NACA TN 3721.)

11. Danberg, James E.: Characteristics of the Turbulent Boundary Layer With Heat and Mass Transfer at $M = 6.7$. NOLTR 64-99, U.S. Navy, Oct. 19, 1964.

12. Danberg, James E.: Measurement of the Characteristics of the Compressible Turbulent Boundary Layer With Air Injection. NAVORD Rep. 6683, U.S. Nav. Ord. Lab., Sept. 3, 1959.

13. Adcock, Jerry B.; Peterson, John B., Jr.; and McRee, Donald I.: Experimental Investigation of a Turbulent Boundary Layer at Mach 6, High Reynolds Numbers, and Zero Heat Transfer. NASA TN D-2907, 1965.

14. Aircraft Div., Douglas Aircraft Co., Inc.: Investigation of Skin Friction Drag on Practical Construction Surfaces for the Supersonic Transport. FDL TDR 64-74, U.S. Air Force, Aug. 1964.

15. Persh, Jerome; and Lee, Roland: Tabulation of Compressible Turbulent Boundary Layer Parameters. NAVORD Rep. 4282 (Aeroballistic Res. Rep. 337), U.S. Nav. Ord. Lab., May 1, 1956.

16. Bertram, Mitchel H.; and Neal, Luther, Jr.: Recent Experiments in Hypersonic Turbulent Boundary Layers. Presented to the AGARD Specialists Meeting on Recent Developments in Boundary-Layer Research (Naples, Italy), May 10-14, 1965.

17. Moore, Dave R.: Velocity Similarity in the Compressible Turbulent Boundary Layer With Heat Transfer. Ph. D. Dissertation, Univ. of Texas, 1962.

TABLE I.- BOUNDARY CONDITIONS FOR EXPERIMENTAL DATA

[Pr = 0.725]

Figure	Reference	M_∞	$T_{t,\infty}$, °K	T_w/T_∞	$\frac{Q}{\rho_\infty u_\infty c_{p,\infty} T_{t,\infty} \theta}$	$\frac{T_w - T_w^*}{T_w^*}$	N	$\frac{(\gamma - 1)M_\infty^2 \frac{c}{a}}{4u_\infty}$
1(a)	5	6.78	639	4.64	0.9239	1.797	5	-2.276
↓	↓	↓	↓	↓	↓	↓	7	-2.017
							9	-1.863
1(b)		5.01	399	4.31	.4680	.332	5	-.512
↓	↓	↓	↓	↓	↓	↓	7	-.441
							9	-.399
2(a)	6	6.00	477	2.210	.5443	-.428	5	3.160
2(b)	↓	3.00	↓	1.316	.4139	-.250	↓	.606
3(a)	7	5.06	562	3.27	.8413	1.230		-1.455
3(b)		5.03	513	3.49	.7765	.961		-1.334
3(c)		5.01	399	4.29	.5197	.437		-.756
3(d)		4.93	325	5.42	.1112	.119		.150
3(e)		5.82	551	4.41	.8554	1.477		-1.740
3(f)		5.79	477	5.35	.6271	.713		-1.493
3(g)		5.75	401	6.19	.3841	.336		-.746
3(h)		6.78	639	4.64	.9306	1.846		-2.333
3(i)		6.78	586	5.22	.8277	1.105		-1.972
3(j)		6.83	586	5.24	.9574	2.690		-3.052
3(k)		6.83	467	6.34	.6986	.774		-1.816
3(l)		7.67	645	5.94	1.0236	4.605		-3.926
3(m)	↓	8.18	655	6.60	1.1542	-18.709		-5.798
4(a)	8	5.11	496	3.511	.4253	-.019		.562
4(b)		5.10	468	3.580	.3612	-.074		.825
4(c)		5.16	476	3.704	.3779	-.039		.702
4(d)		5.12	465	3.761	.3267	-.079		.866
4(e)		5.20	467	3.769	.3715	-.046		.730
4(f)		4.98	383	4.511	.2810	.098		.211
4(g)		5.18	399	4.726	.4807	.401		.754
4(h)		5.20	374	4.807	.3631	.201		-.173
4(i)		5.24	384	4.971	.2692	.0954		.249
4(j)		5.24	379	5.019	.3200	.175		.071
4(k)		5.21	383	5.145	.5192	.594		-1.298
4(l)		5.20	366	5.374	.3635	.343		-.683
4(m)		5.26	364	5.463	.4760	.565		-1.291
4(n)	↓	5.29	363	5.564	.1804	.098		.277
5(a)	9	1.974	310	1.687	-.0092	-.014		.152
5(b)		1.989	316	1.702	.0799	.066		.008
5(c)		1.994	304	1.720	.0060	.010		.111
5(d)		1.969	297	1.731	.0113	.030		.075
5(e)		2.273	299	1.915	.0723	.060		.045
5(f)		2.306	293	1.975	.0498	.053		.059
5(g)		2.328	294	1.976	.0748	.068		.035
5(h)	↓	3.035	286	2.639	.0827	.068	↓	.107

TABLE I.- BOUNDARY CONDITIONS FOR EXPERIMENTAL DATA – Concluded

[Pr = 0.725]

Figure	Reference	M_∞	$T_{t,\infty}$, °K	T_w/T_∞	$\frac{Q}{\rho_\infty u_\infty c_{p,\infty} T_{t,\infty} \theta}$	$\frac{T_w - T_w^*}{T_w^*}$	N	$\frac{(\gamma - 1)M_\infty^2 \frac{c}{a}}{4u_\infty}$
6(a)	9	4.161	313	4.236	0.0860	0.115	5	0.092
6(b)	↓	4.238	314	4.260	.2618	.307	↓	-.493
6(c)	11	3.035	291	2.668	.0547	.055		.143
6(d)	12	6.500	550	4.100	.7338	.369		-.450
7(a)	13	5.07	369	4.595	.2958	.106		.192
7(b)		5.20	383	4.615	.3289	.110		.186
7(c)		5.02	377	5.085	.3473	.326		-.586
7(d)		5.18	379	5.210	.2346	.129		.122
8(a)		6.02	≈539	5.16	.6273	.556		-1.109
8(b)		↓	↓	↓	.8231	1.554		-2.439
8(c)	↓				.7272	.944	↓	-1.788
8(d)	14		483	7.38	.0215	.001	5	1.016
	↓	↓	↓	↓	↓	↓	20	.830
9(a)	15	.85	315	.997	.0456	-.083	5	.110
9(b)			346	1.015	.0268	-.081		.112
9(c)			333	1.031	.0364	-.059		.086
9(d)			329	1.037	.0399	-.051		.076
9(e)			315	1.042	.0458	-.042		.064
9(f)			322	1.059	.0364	-.034		.057
9(g)			324	1.064	.0307	-.034		.058
9(h)			321	1.071	.0309	-.027		.051
9(i)			320	1.073	.0393	-.019		.040
9(j)			322	1.077	.0446	-.011		.030
9(k)			315	1.086	.0305	-.014		.036
9(l)		↓	329	1.092	.0336	-.006		.026
9(m)		1.98	335	1.539	.2291	.120		-.082
9(n)			330	1.572	.1897	.098		-.050
9(o)			327	1.630	.2352	.194		-.182
9(p)			308	1.647	.0527	.011		.099
9(q)			310	1.685	.0572	.039		.054
9(r)		↓	305	1.700	.1963	.196		-.187
9(s)		2.98	326	2.189	.2617	.089		.028
9(t)			329	2.271	.1890	.045		.130
9(u)			320	2.308	.1929	.067		.084
9(v)			333	2.370	.1163	.015		.213
9(w)			323	2.470	.3986	.451		-.575
9(x)			316	2.478	.1823	.134		-.053
9(y)			335	2.490	.4380	.542		-.691
9(z)			333	2.510	.5365	.801		-.951
9(aa)		↓	310	2.542	-.0307	-.047		.411
9(bb)		4.88	389	3.928	.3765	.113		.133
9(cc)			369	4.135	.5781	.596		-1.039
9(dd)			394	4.190	.4020	.229		-.231
9(ee)	↓	↓	394	4.250	.3371	.145	↓	.031

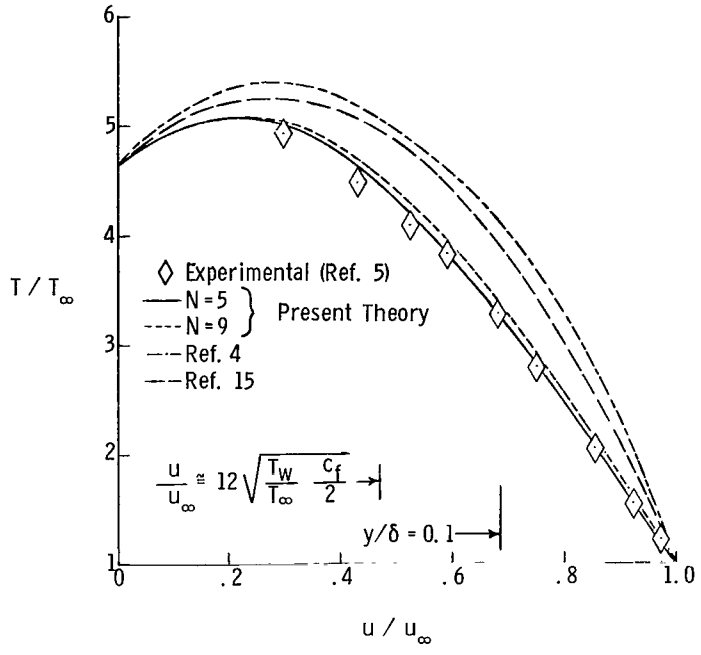

(a) $M_\infty = 6.78$; $T_w/T_\infty = 4.64$.

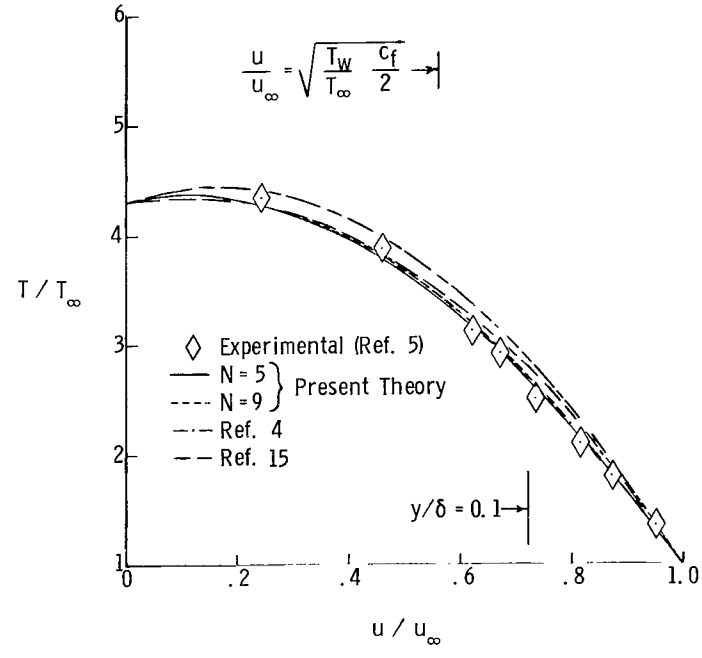

(b) $M_\infty = 5.01$; $T_w/T_\infty = 4.31$.

Figure 1.- Experimental temperature-velocity profile data obtained from reference 5 compared with theoretical results calculated by using the methods of the present paper, reference 4, and reference 15.

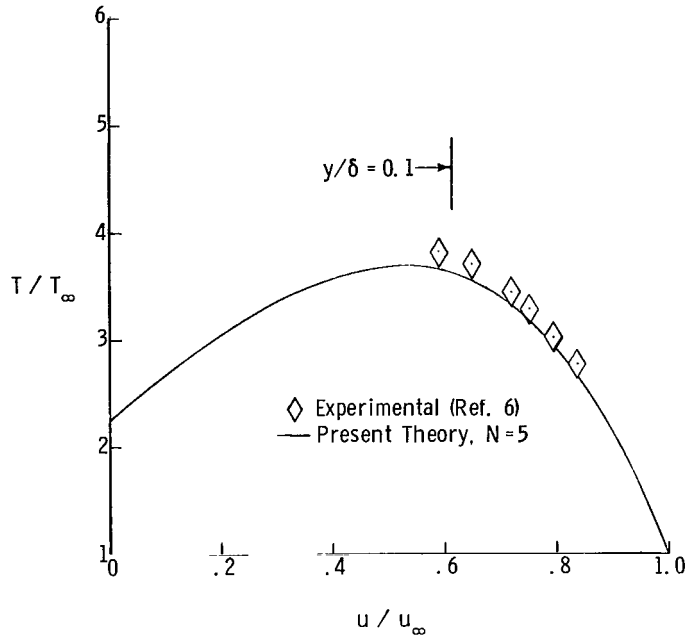

(a) $M_\infty = 6.00$; $T_W/T_\infty = 2.210$.

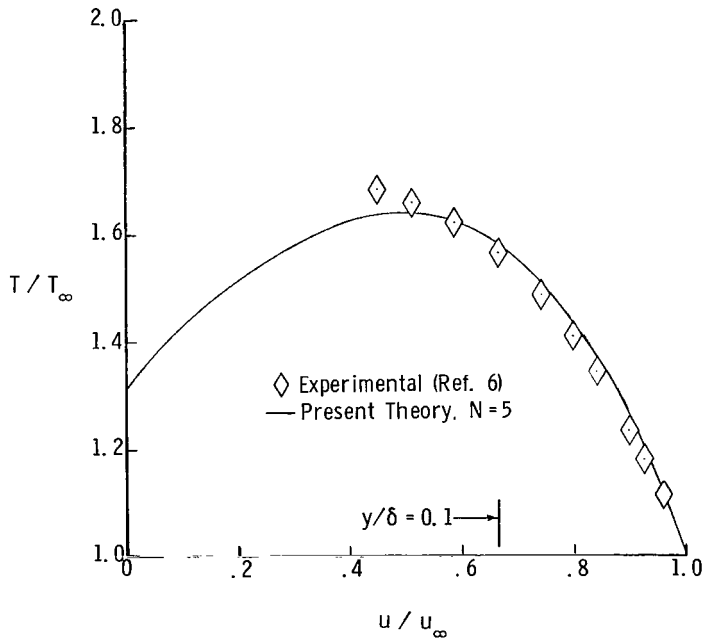

(b) $M_\infty = 3.00$; $T_W/T_\infty = 1.316$.

Figure 2.- Experimental temperature-velocity profile data obtained from reference 6 compared with the present theoretical results.

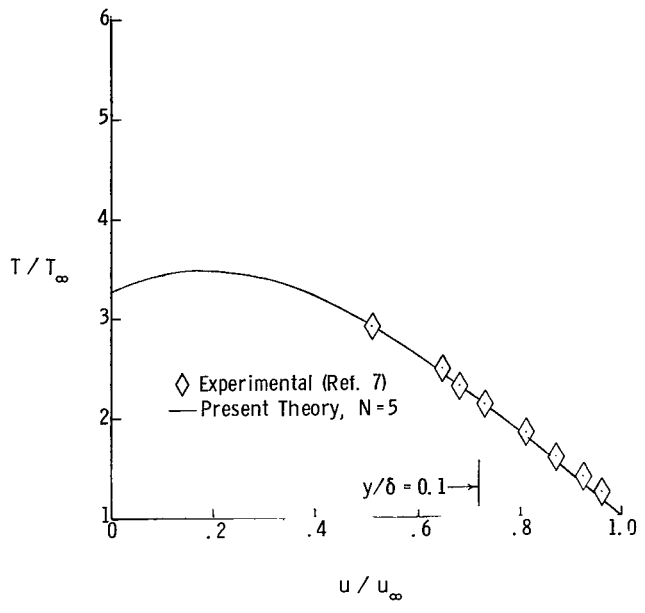

(a) $M_\infty = 5.06$; $T_w/T_\infty = 3.27$.

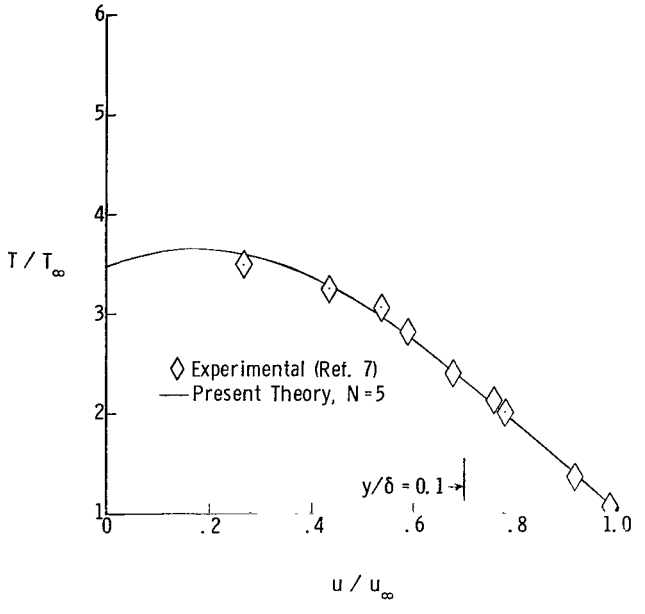

(b) $M_\infty = 5.03$; $T_w/T_\infty = 3.49$.

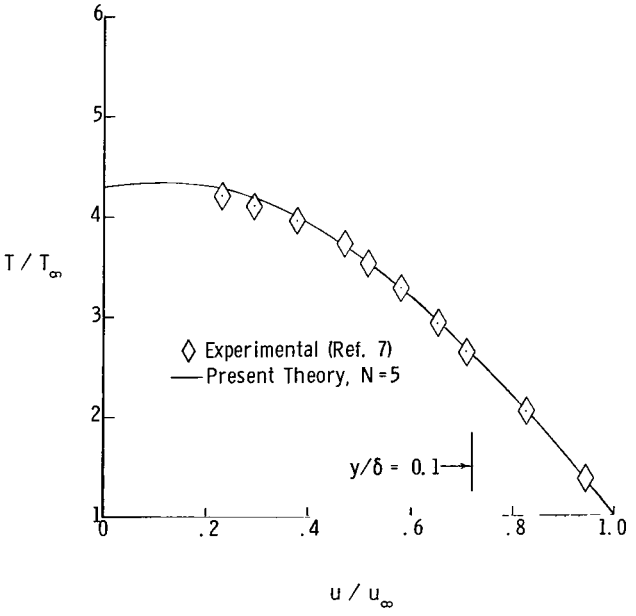

(c) $M_\infty = 5.01$; $T_w/T_\infty = 4.29$.

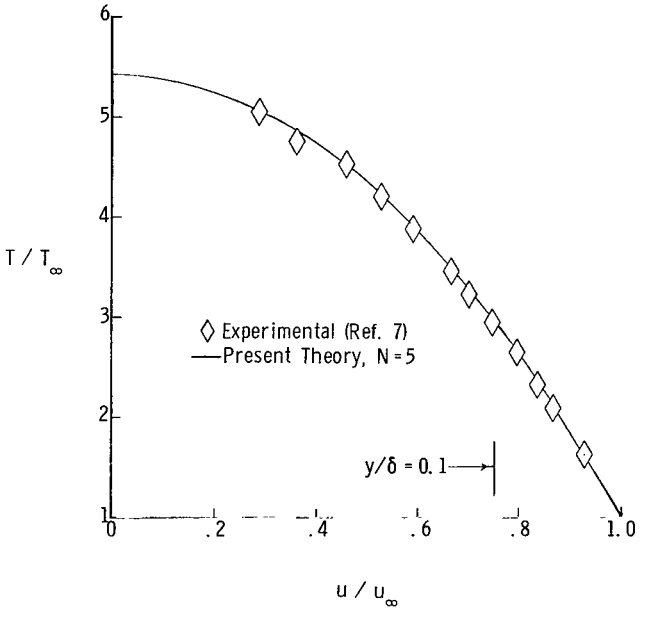

(d) $M_\infty = 4.93$; $T_w/T_\infty = 5.42$.

Figure 3.- Experimental temperature-velocity profile data obtained from reference 7 compared with the present theoretical results.

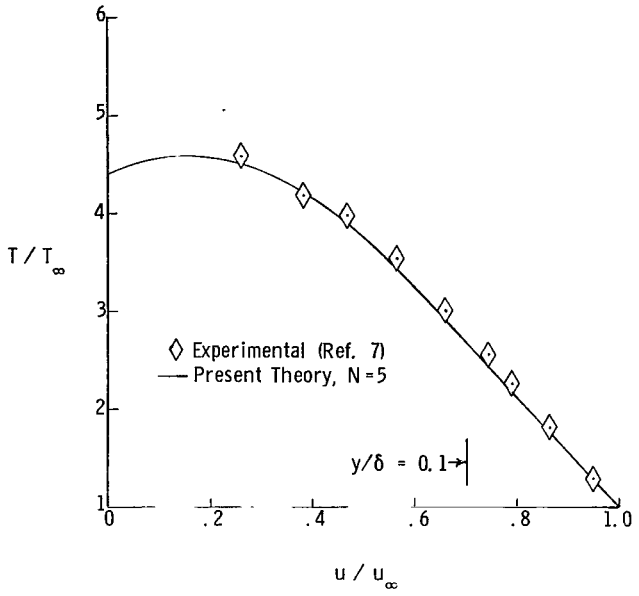

(e) $M_\infty = 5.82$; $T_w/T_\infty = 4.41$.

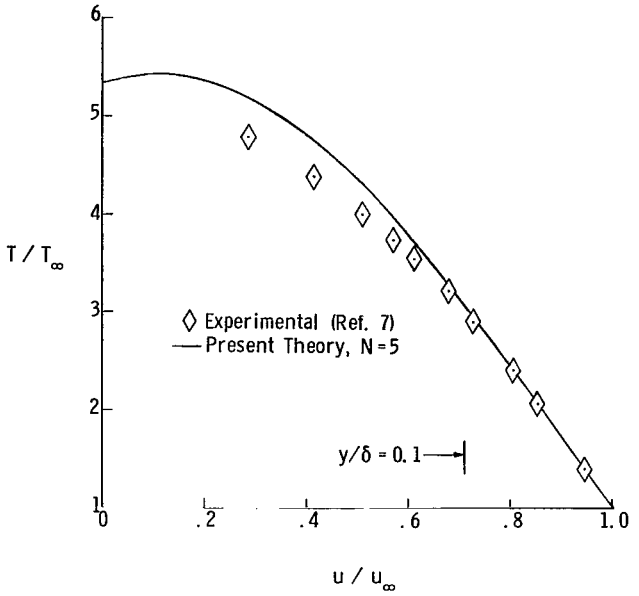

(f) $M_\infty = 5.79$; $T_w/T_\infty = 5.35$.

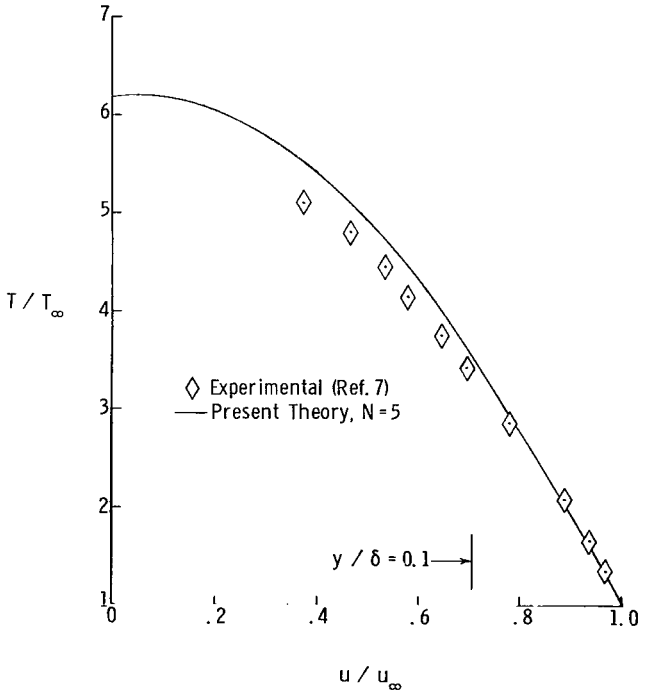

(g) $M_\infty = 5.75$; $T_w/T_\infty = 6.19$.

Figure 3.- Continued.

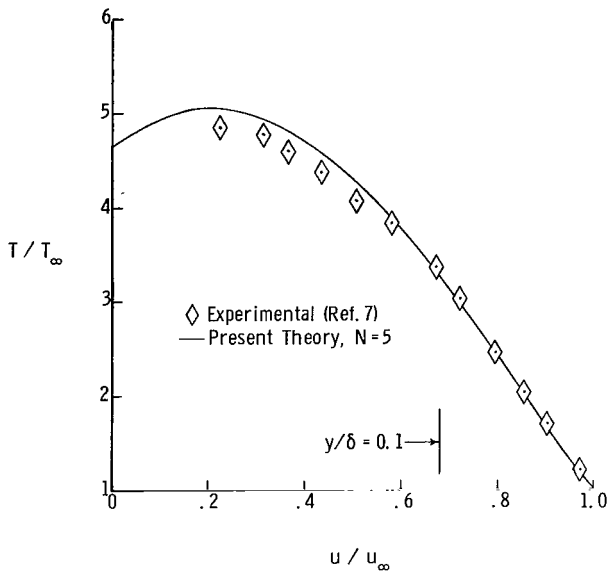

(h) $M_\infty = 6.78$; $T_W/T_\infty = 4.64$.

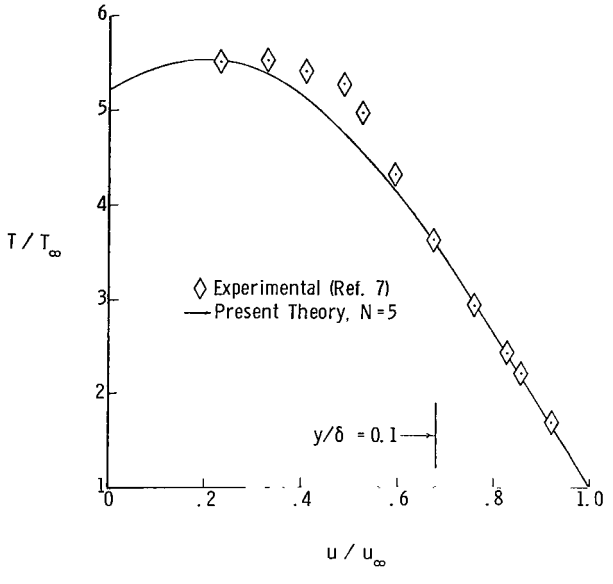

(i) $M_\infty = 6.78$; $T_W/T_\infty = 5.22$.

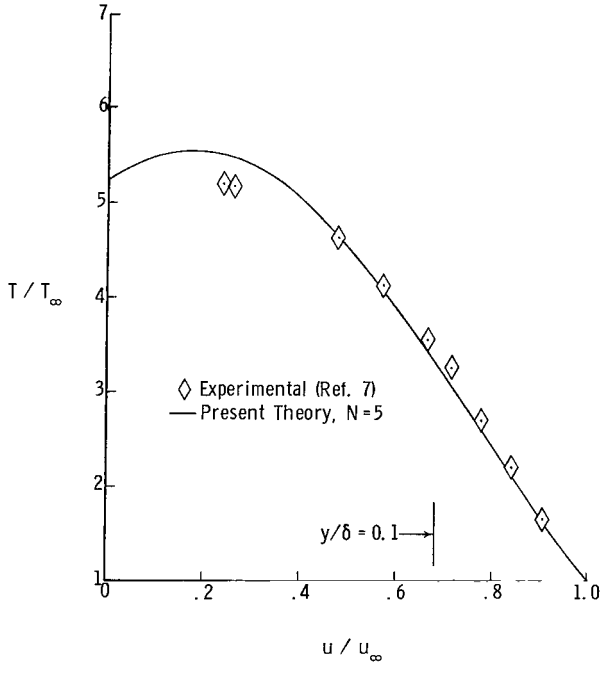

(j) $M_\infty = 6.83$; $T_W/T_\infty = 5.24$.

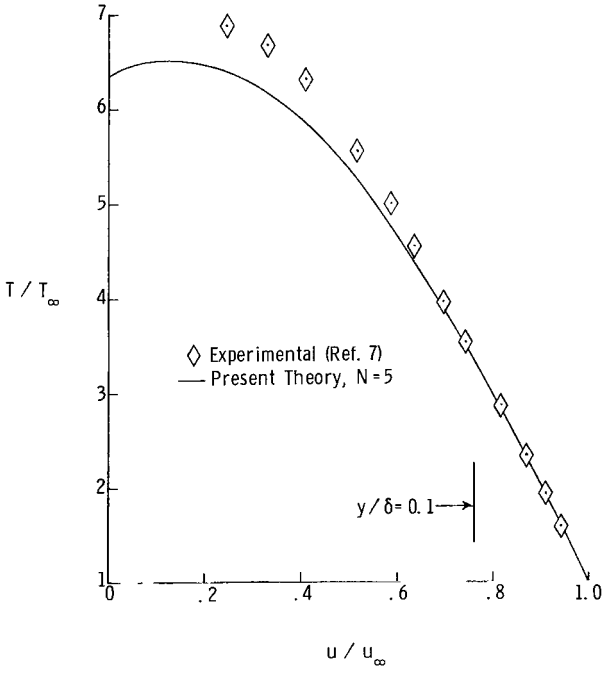

(k) $M_\infty = 6.83$; $T_W/T_\infty = 6.34$.

Figure 3.- Continued.

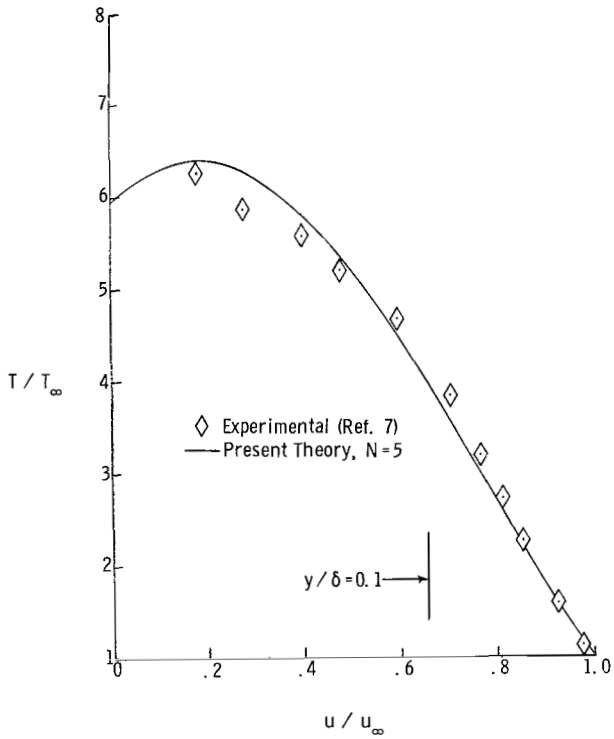

(l) $M_\infty = 7.67$; $T_W/T_\infty = 5.94$.

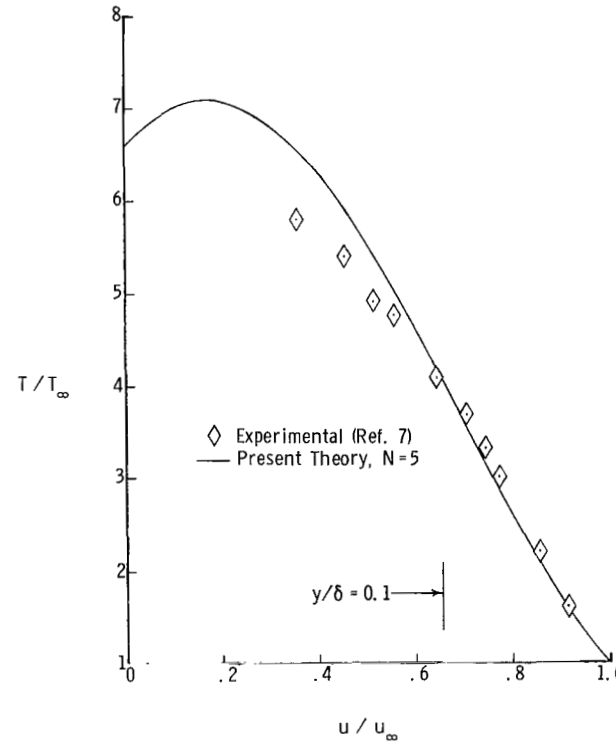

(m) $M_\infty = 8.18$; $T_W/T_\infty = 6.60$.

Figure 3.- Concluded.

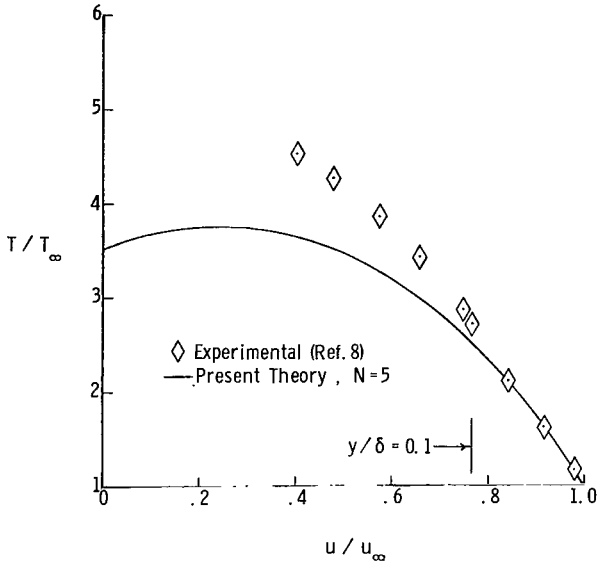

(a) $M_\infty = 5.11$; $T_W/T_\infty = 3.511$.

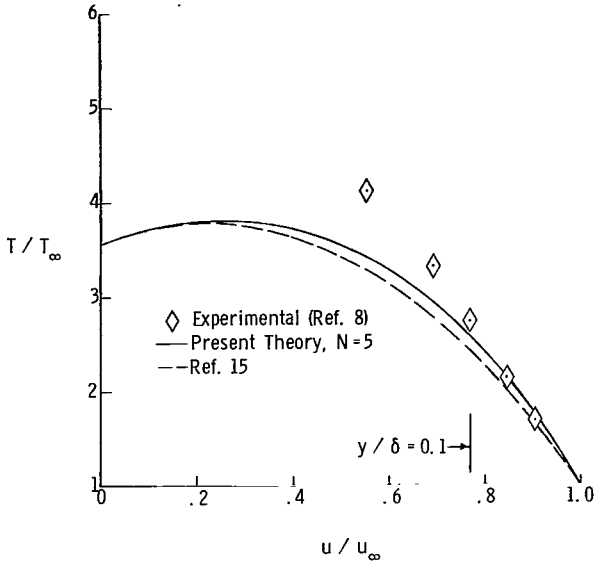

(b) $M_\infty = 5.10$; $T_W/T_\infty = 3.580$.

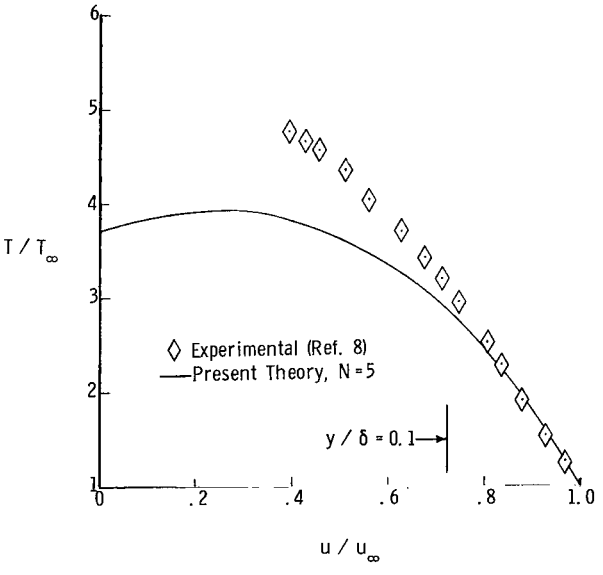

(c) $M_\infty = 5.16$; $T_W/T_\infty = 3.704$.

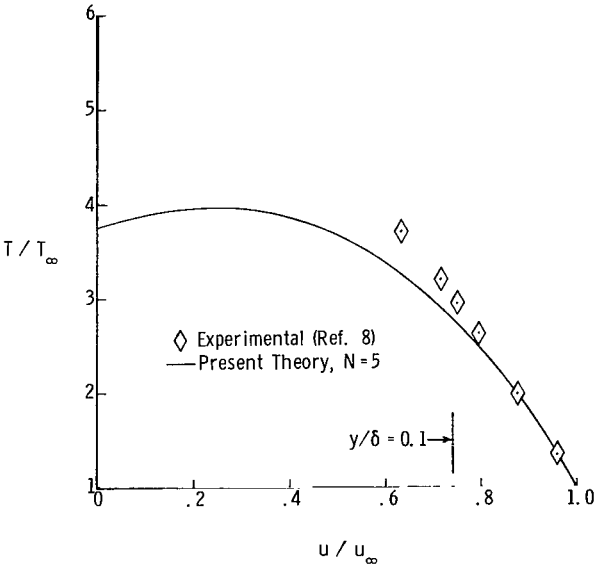

(d) $M_\infty = 5.12$; $T_W/T_\infty = 3.761$.

Figure 4.- Experimental temperature-velocity data obtained from reference 8 compared with theoretical results calculated by using the method of the present paper.

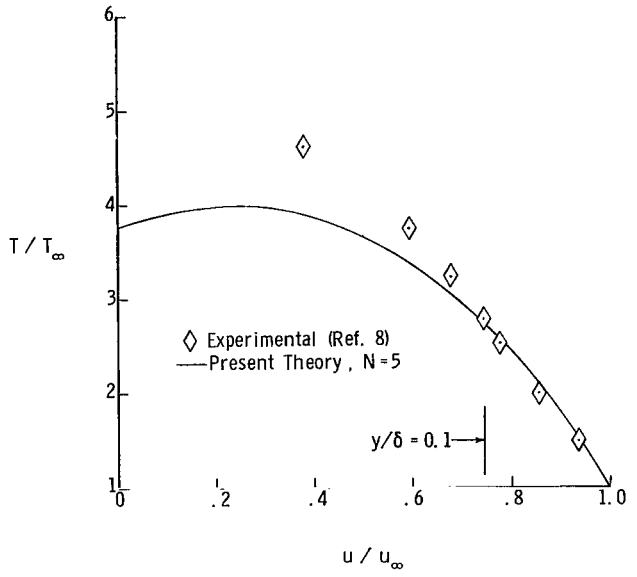

(e) $M_\infty = 5.20$; $T_w/T_\infty = 3.769$.

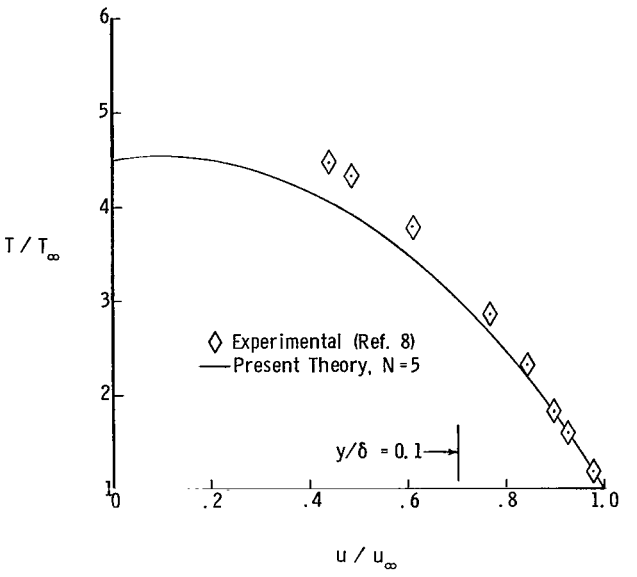

(f) $M_\infty = 4.98$; $T_w/T_\infty = 4.511$.

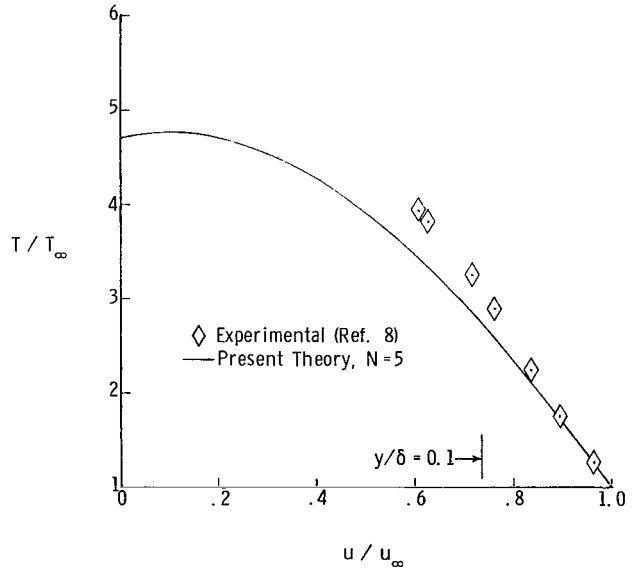

(g) $M_\infty = 5.18$; $T_w/T_\infty = 4.726$.

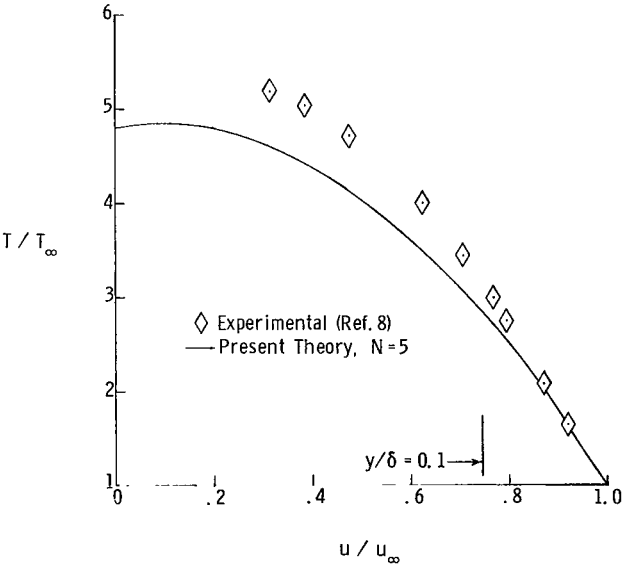

(h) $M_\infty = 5.20$; $T_w/T_\infty = 4.807$.

Figure 4.- Continued.

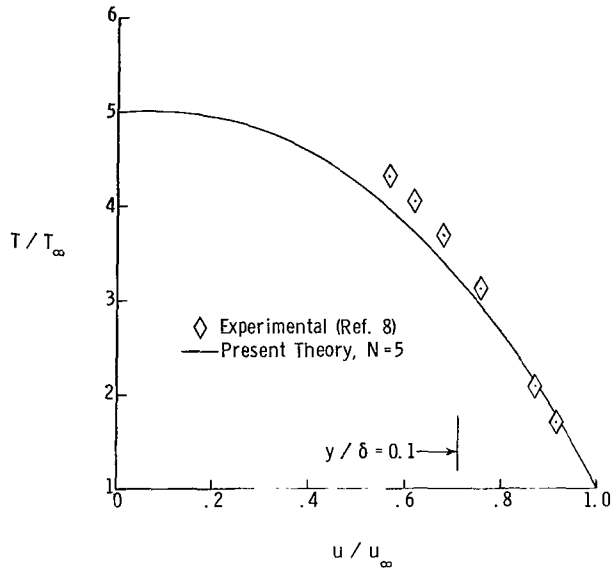

(i) $M_\infty = 5.24$; $T_W/T_\infty = 4.971$.

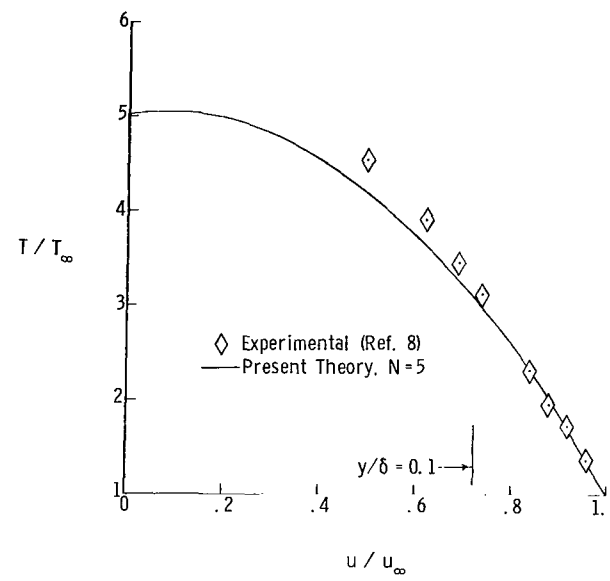

(j) $M_\infty = 5.24$; $T_W/T_\infty = 5.019$.

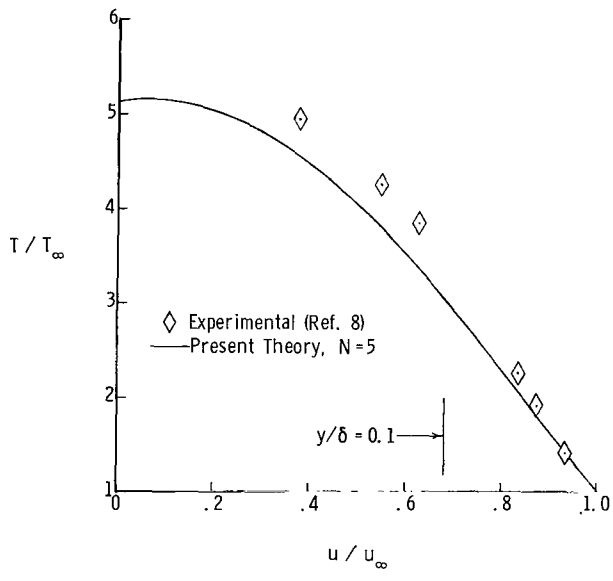

(k) $M_\infty = 5.21$; $T_W/T_\infty = 5.145$.

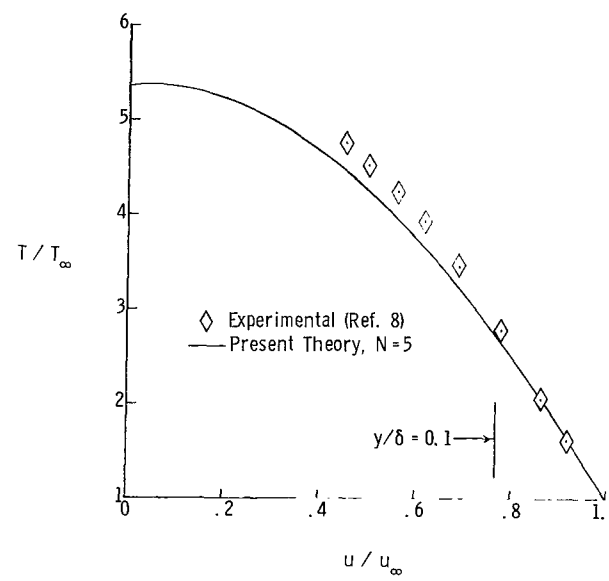

(l) $M_\infty = 5.20$; $T_W/T_\infty = 5.374$.

Figure 4.- Continued.

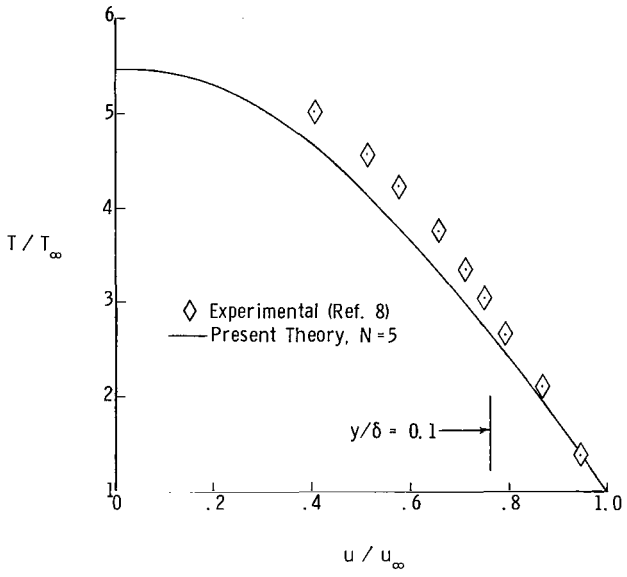

(m) $M_\infty = 5.26$; $T_W/T_\infty = 5.463$.

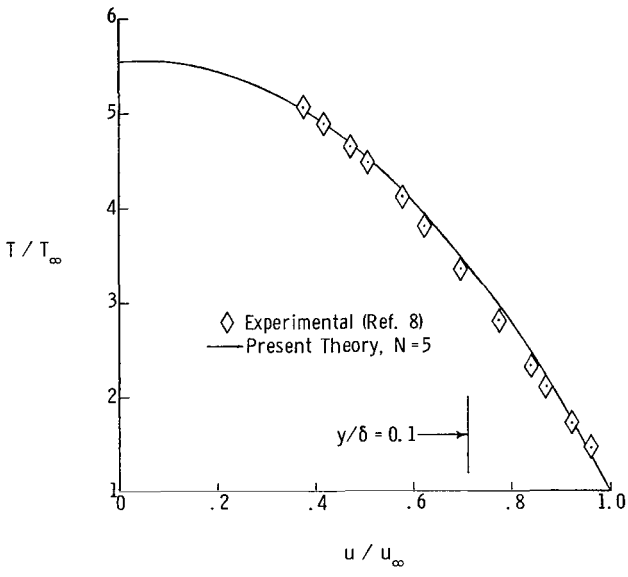

(n) $M_\infty = 5.29$; $T_W/T_\infty = 5.564$.

Figure 4.- Concluded.

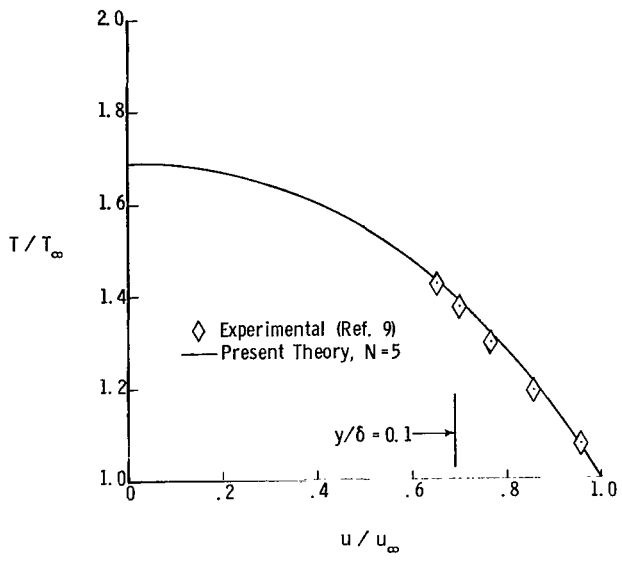

(a) $M_\infty = 1.974$; $T_w/T_\infty = 1.687$.

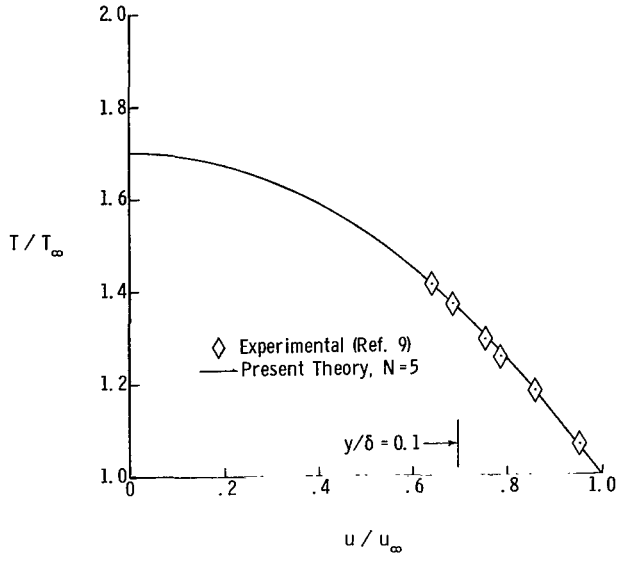

(b) $M_\infty = 1.989$; $T_w/T_\infty = 1.702$.

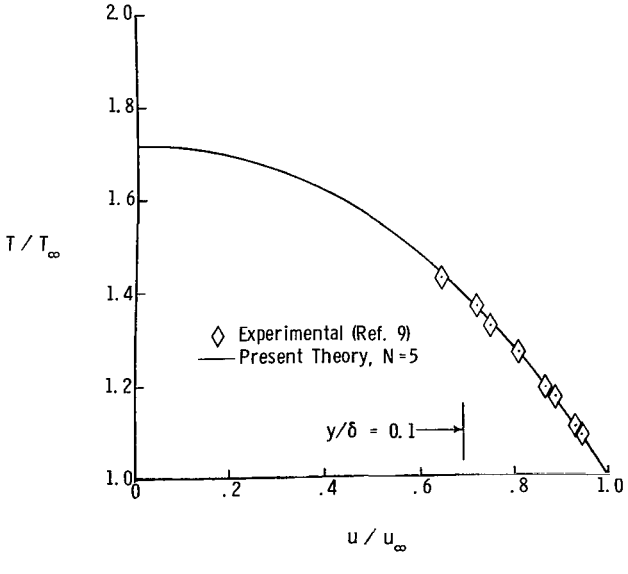

(c) $M_\infty = 1.994$; $T_w/T_\infty = 1.720$.

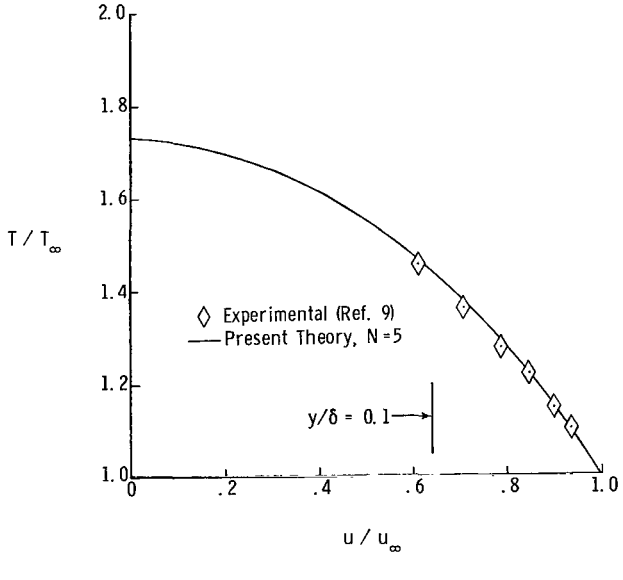

(d) $M_\infty = 1.968$; $T_w/T_\infty = 1.731$.

Figure 5.- Experimental temperature-velocity profile data obtained from reference 9 compared with the present theoretical results.

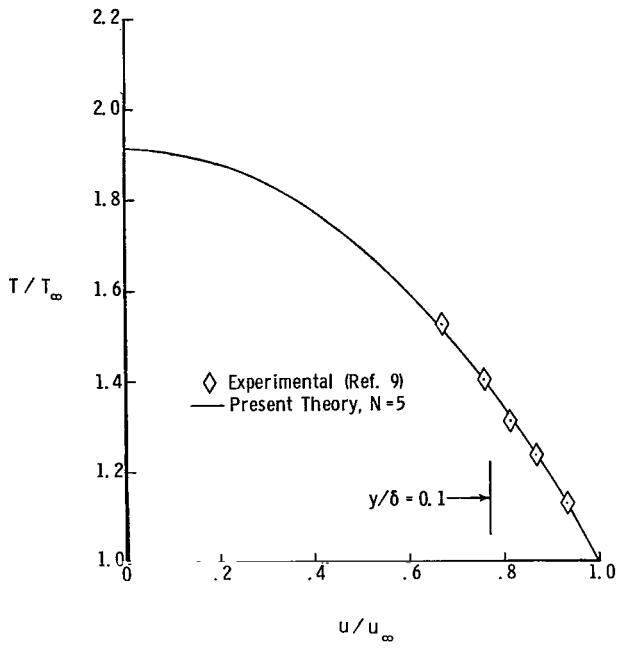

(e) $M_\infty = 2.273$; $T_W/T_\infty = 1.915$.

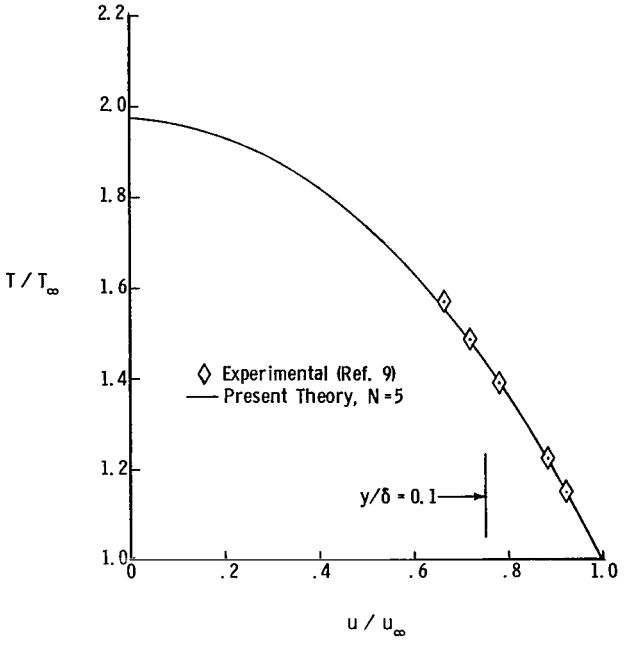

(f) $M_\infty = 2.306$; $T_W/T_\infty = 1.975$.

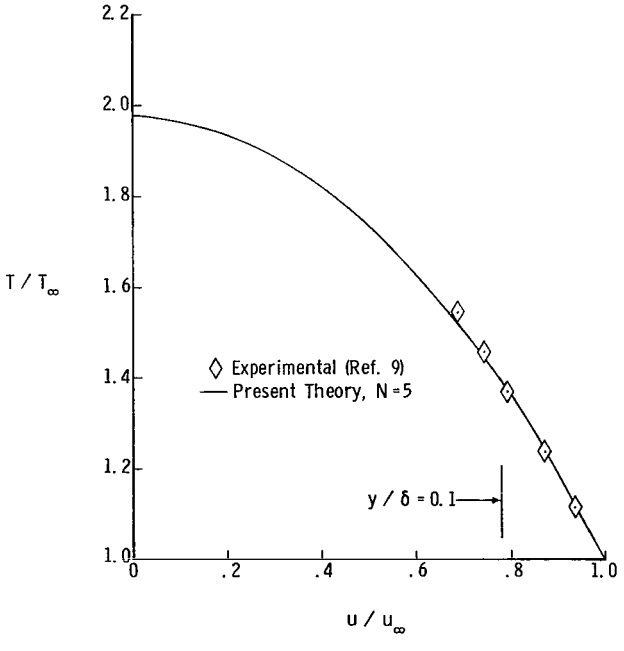

(g) $M_\infty = 2.328$; $T_W/T_\infty = 1.976$.

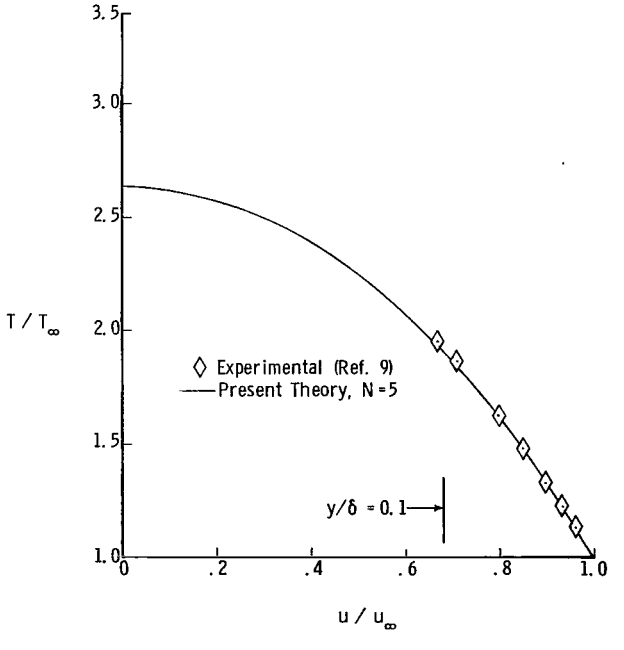

(h) $M_\infty = 3.035$; $T_W/T_\infty = 2.639$.

Figure 5.- Concluded.

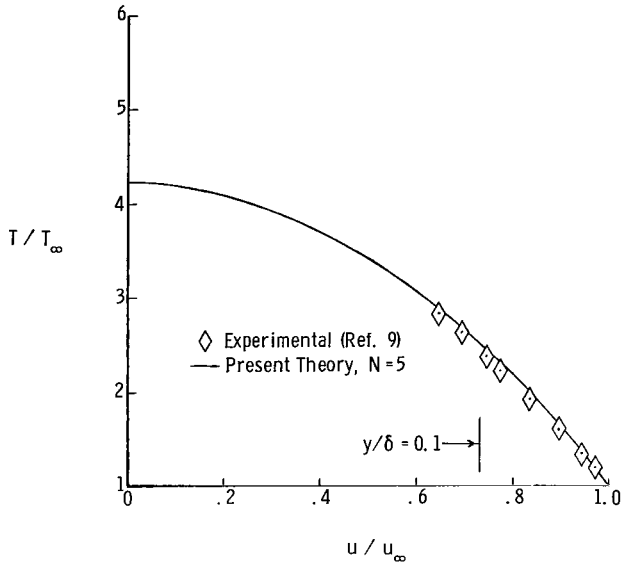

(a) $M_\infty = 4.161$; $T_W/T_\infty = 4.236$.

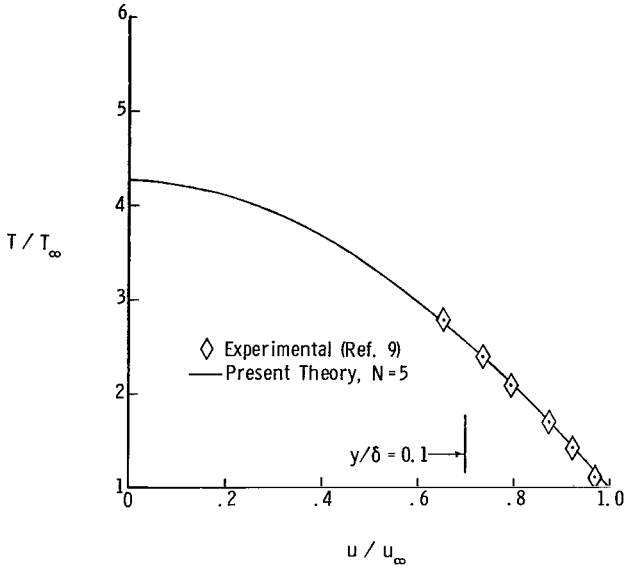

(b) $M_\infty = 4.238$; $T_W/T_\infty = 4.260$.

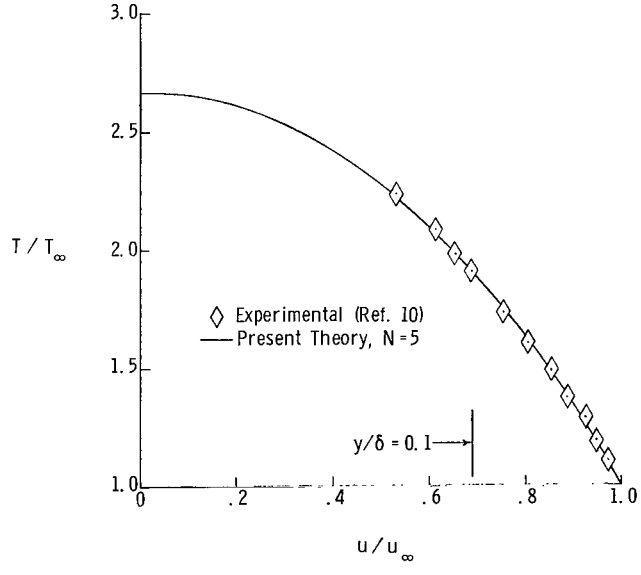

(c) $M_\infty = 3.035$; $T_W/T_\infty = 2.668$.

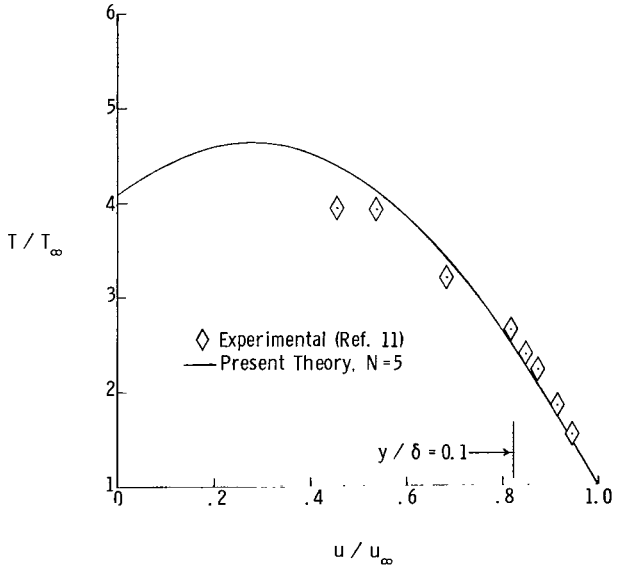

(d) $M_\infty = 6.500$; $T_W/T_\infty = 4.100$.

Figure 6.- Experimental temperature-velocity profile data obtained from references 9, 10, and 11 compared with the present theoretical results.

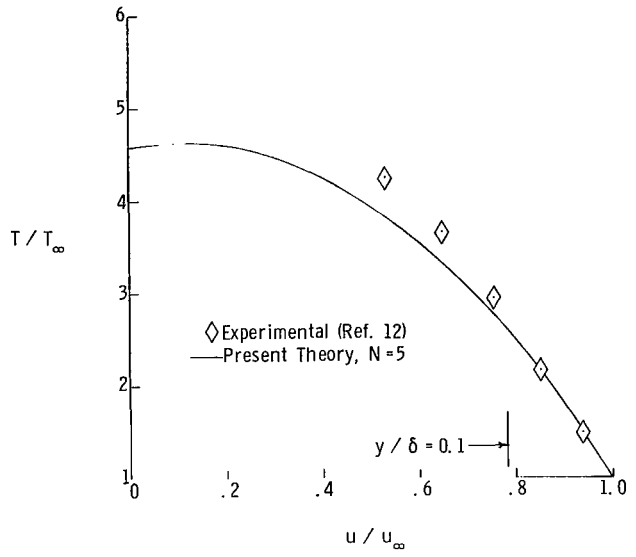

(a) $M_\infty = 5.07$; $T_W/T_\infty = 4.595$.

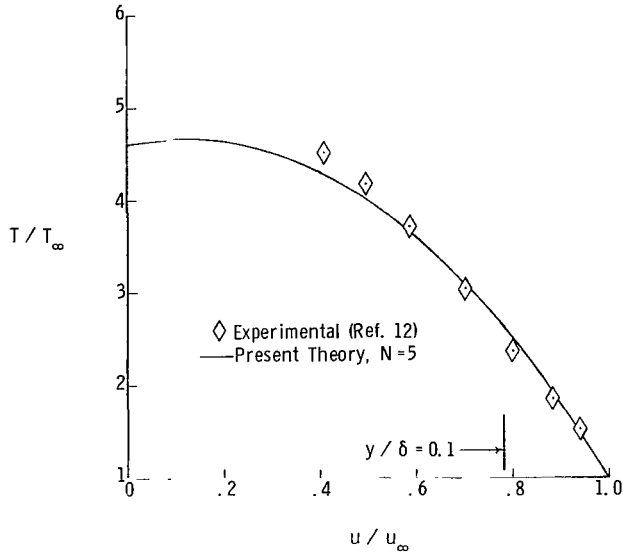

(b) $M_\infty = 5.20$; $T_W/T_\infty = 4.615$.

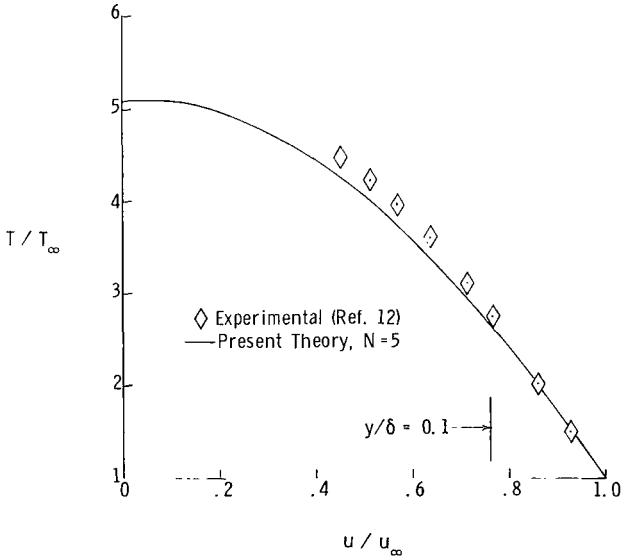

(c) $M_\infty = 5.02$; $T_W/T_\infty = 5.085$.

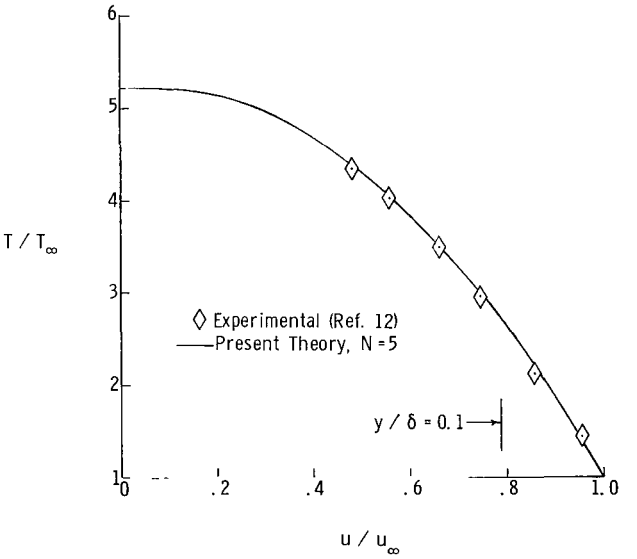

(d) $M_\infty = 5.18$; $T_W/T_\infty = 5.210$.

Figure 7.- Experimental temperature-velocity profile data obtained from reference 12 compared with the present theoretical results.

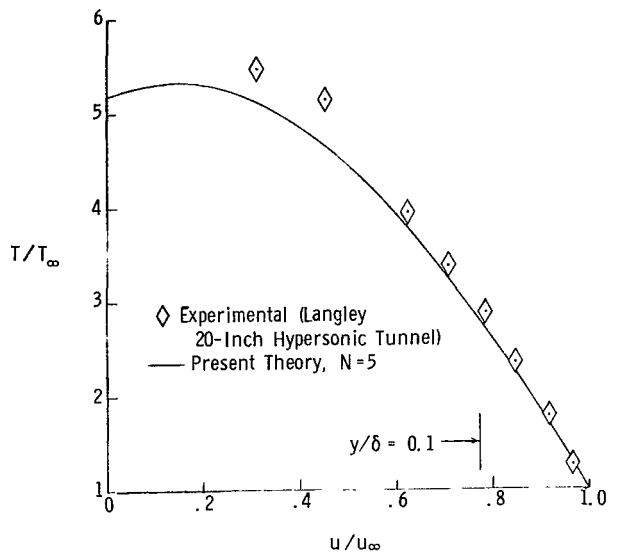

(a) $M_\infty = 6.02$; $T_W/T_\infty = 5.16$.

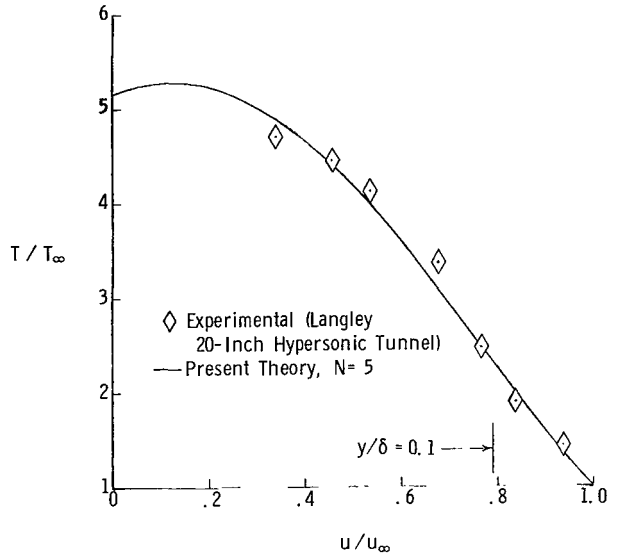

(b) $M_\infty = 6.02$; $T_W/T_\infty = 5.16$.

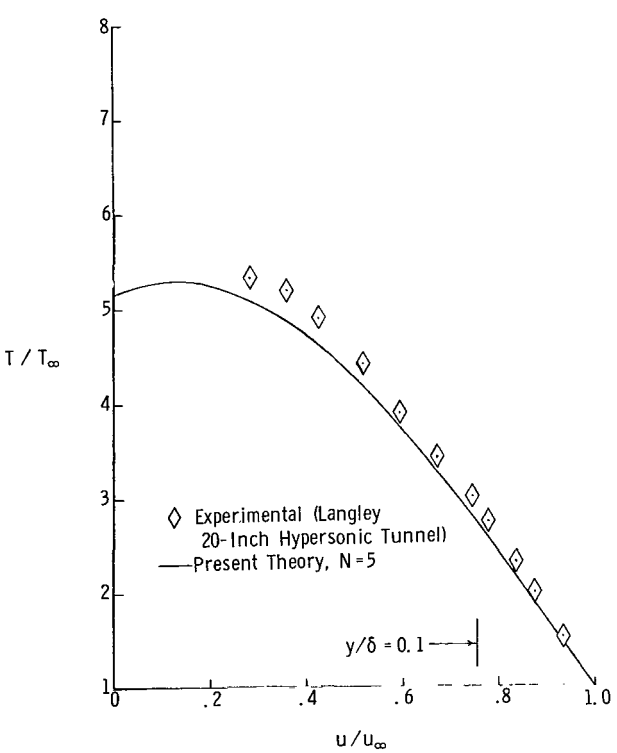

(c) $M_\infty = 6.02$; $T_W/T_\infty = 5.16$.

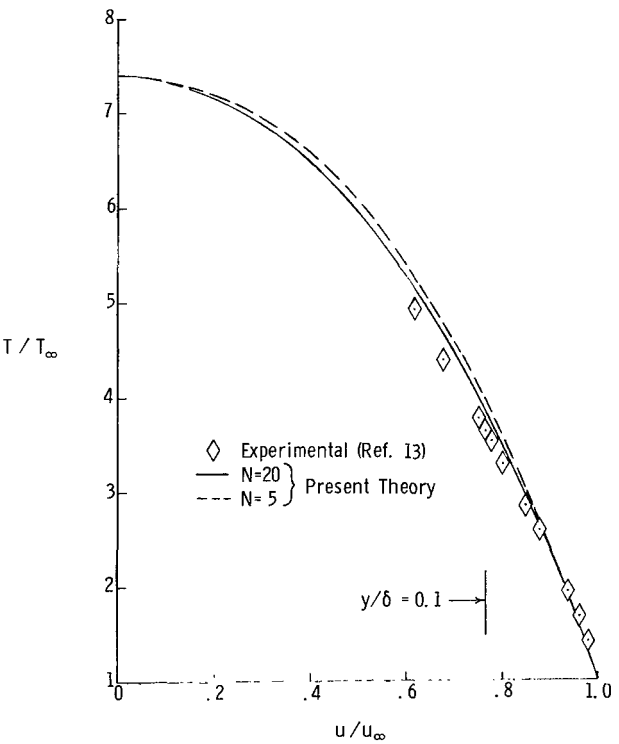

(d) $M_\infty = 6.02$; $T_W/T_\infty = 7.38$.

Figure 8.- Experimental temperature-velocity profile data obtained in the Langley 20-inch hypersonic tunnel and experimental data obtained from reference 13 compared with the present theoretical results.

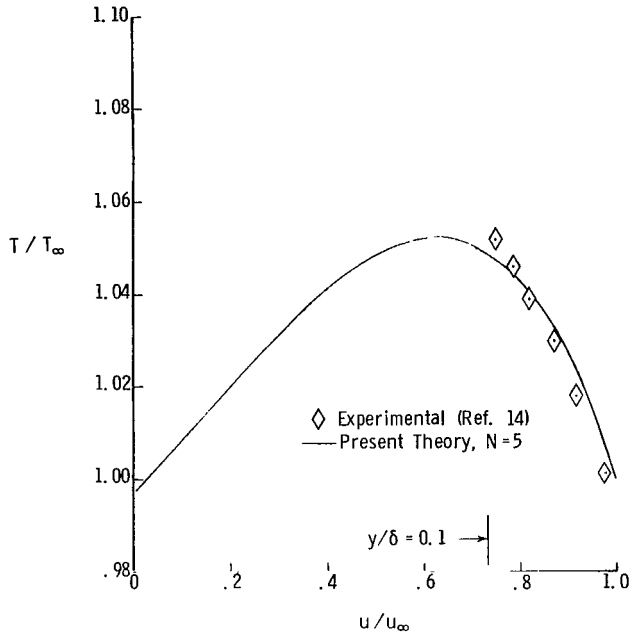

(a) $M_\infty = 0.85$; $T_w/T_\infty = 0.997$.

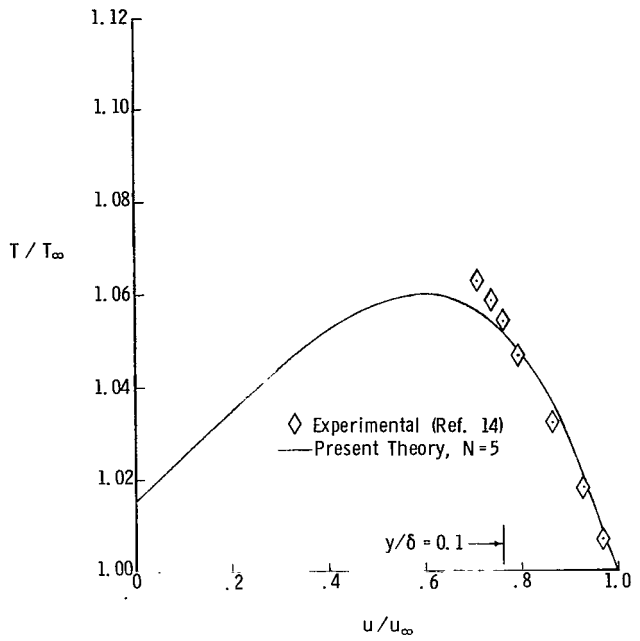

(b) $M_\infty = 0.85$; $T_w/T_\infty = 1.015$.

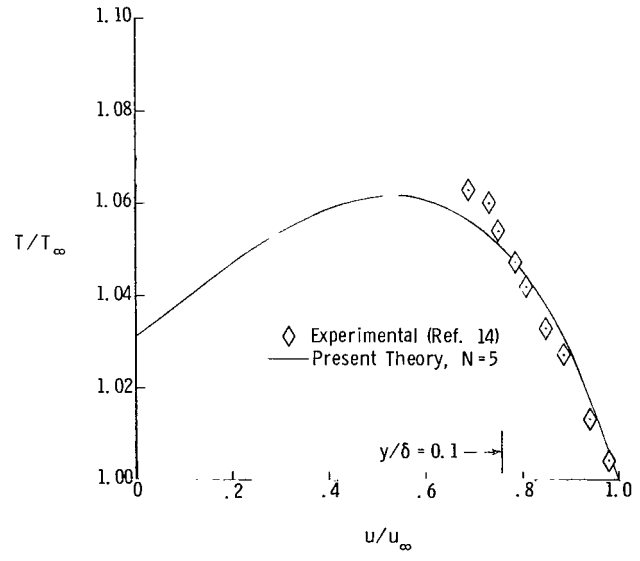

(c) $M_\infty = 0.85$; $T_w/T_\infty = 1.031$.

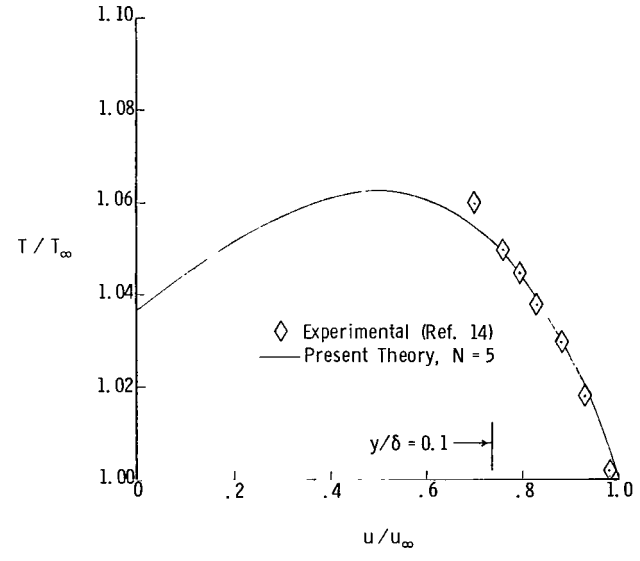

(d) $M_\infty = 0.85$; $T_w/T_\infty = 1.037$.

Figure 9.- Experimental temperature-velocity profile data obtained from reference 14 compared with the present theoretical results.

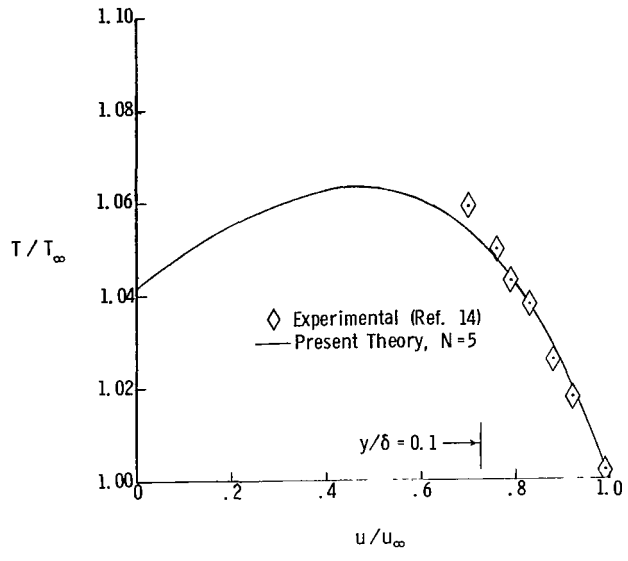

(e) $M_\infty = 0.85$; $T_w/T_\infty = 1.042$.

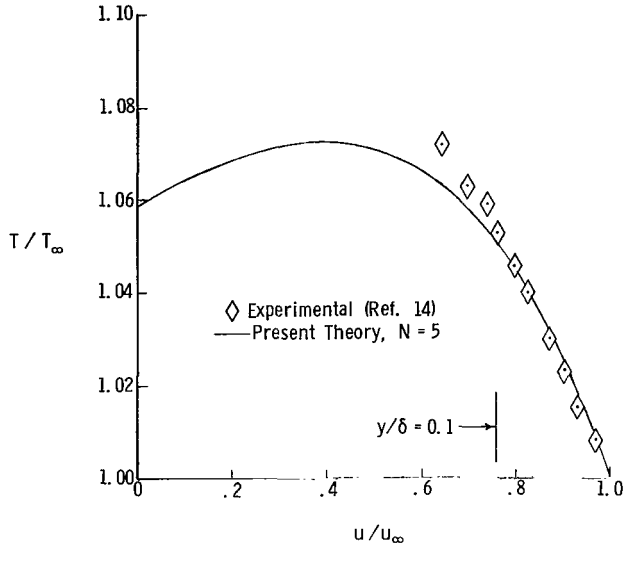

(f) $M_\infty = 0.85$; $T_w/T_\infty = 1.059$.

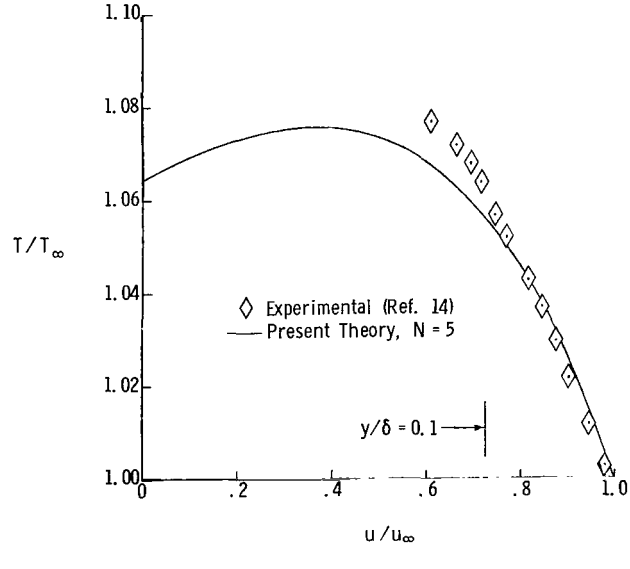

(g) $M_\infty = 0.85$; $T_w/T_\infty = 1.064$.

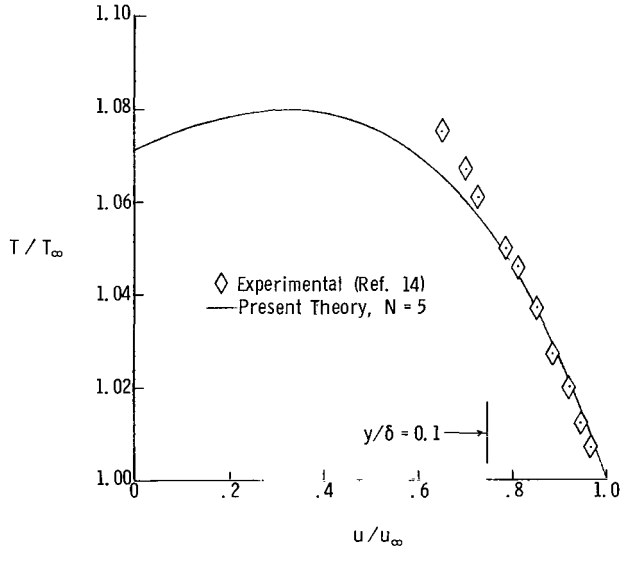

(h) $M_\infty = 0.85$; $T_w/T_\infty = 1.071$.

Figure 9.- Continued.

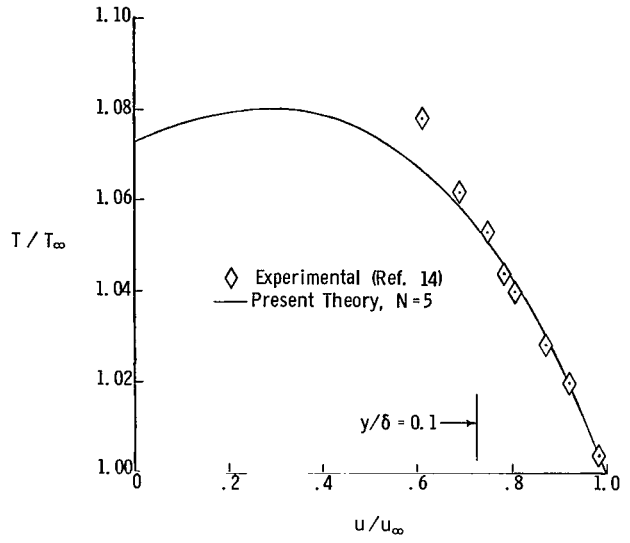

(i) $M_\infty = 0.85$; $T_W/T_\infty = 1.073$.

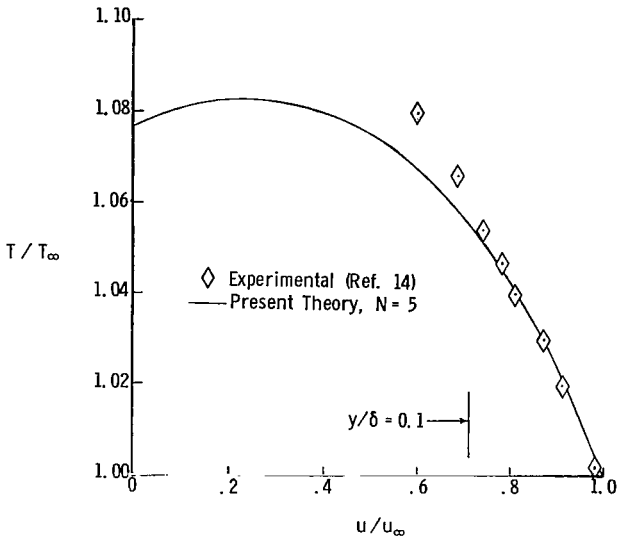

(j) $M_\infty = 0.85$; $T_W/T_\infty = 1.077$.

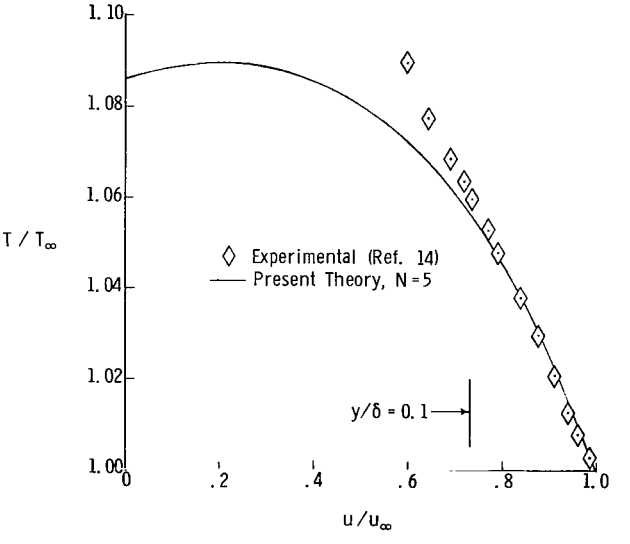

(k) $M_\infty = 0.85$; $T_W/T_\infty = 1.086$.

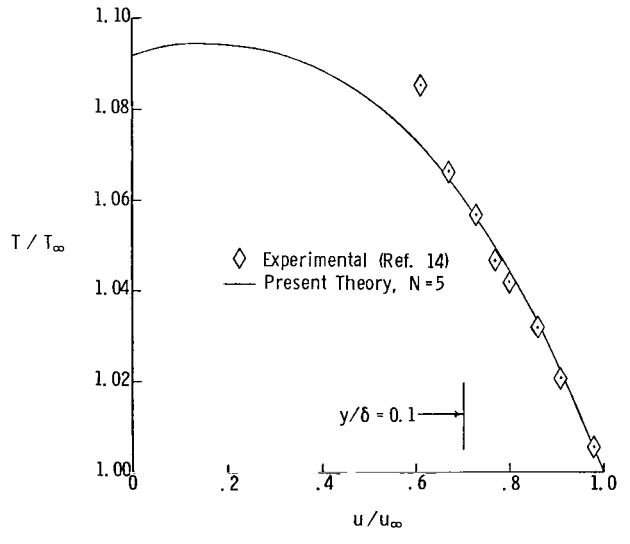

(l) $M_\infty = 0.85$; $T_W/T_\infty = 1.092$.

Figure 9.- Continued.

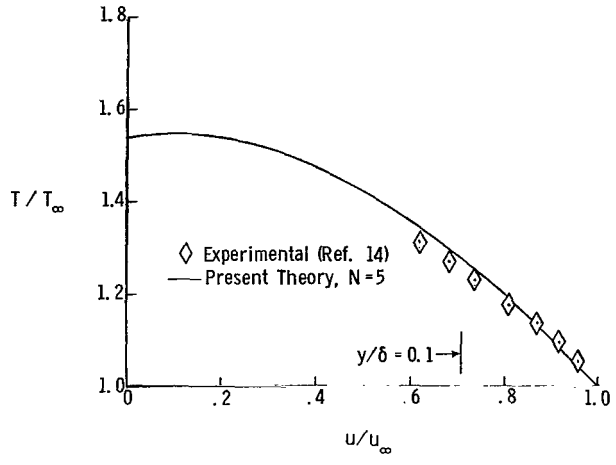

(m) $M_\infty = 1.98$; $T_W/T_\infty = 1.539$.

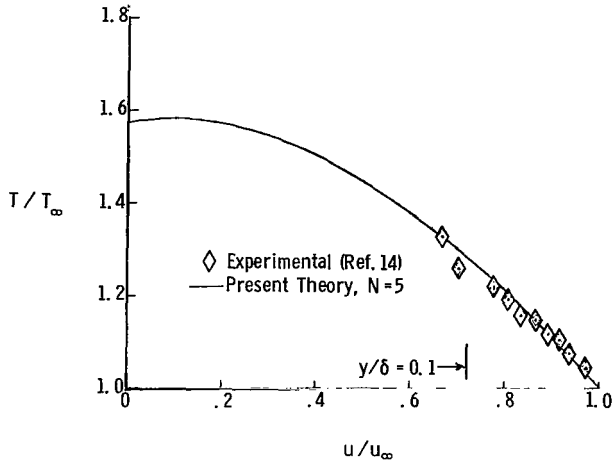

(n) $M_\infty = 1.98$; $T_W/T_\infty = 1.572$.

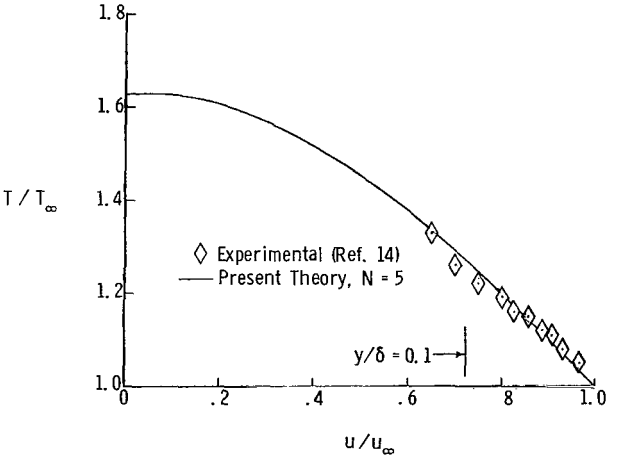

(o) $M_\infty = 1.98$; $T_W/T_\infty = 1.630$.

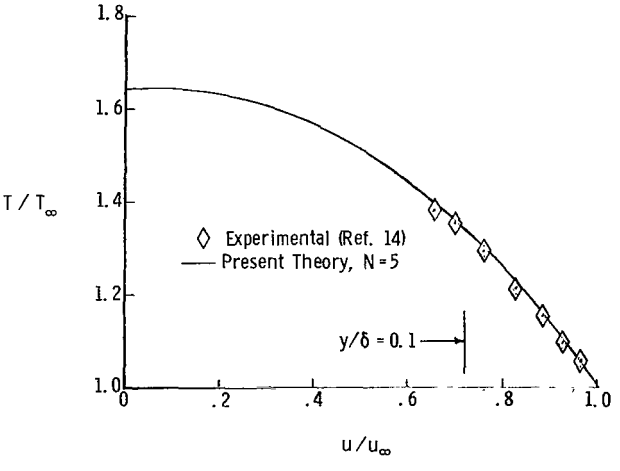

(p) $M_\infty = 1.98$; $T_W/T_\infty = 1.647$.

Figure 9.- Continued.

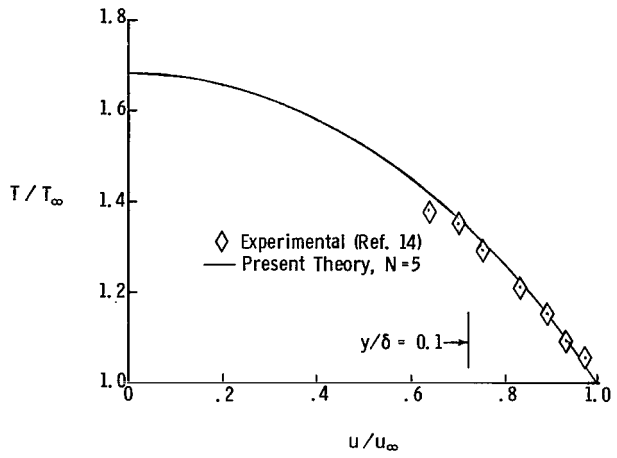

(q) $M_\infty = 1.98$; $T_W/T_\infty = 1.685$.

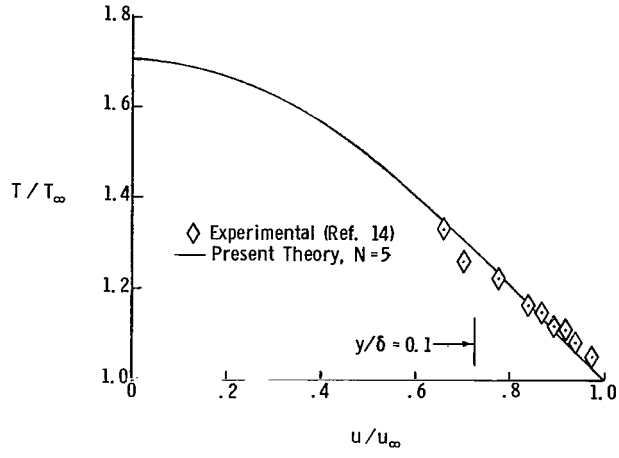

(r) $M_\infty = 1.98$; $T_W/T_\infty = 1.700$.

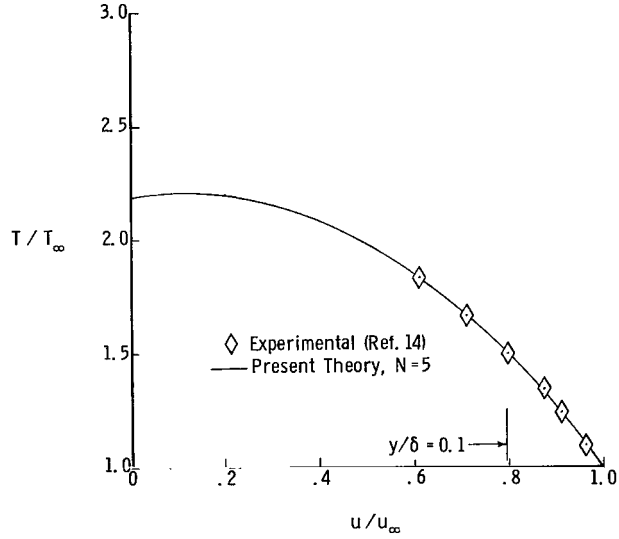

(s) $M_\infty = 2.98$; $T_W/T_\infty = 2.189$.

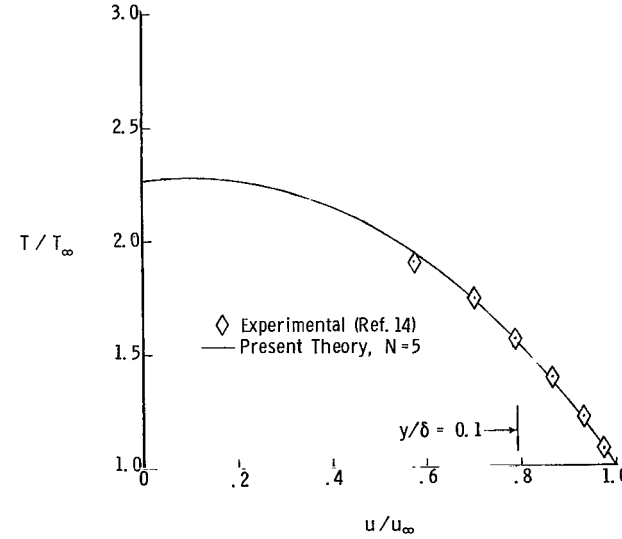

(t) $M_\infty = 2.98$; $T_W/T_\infty = 2.271$.

Figure 9.- Continued.

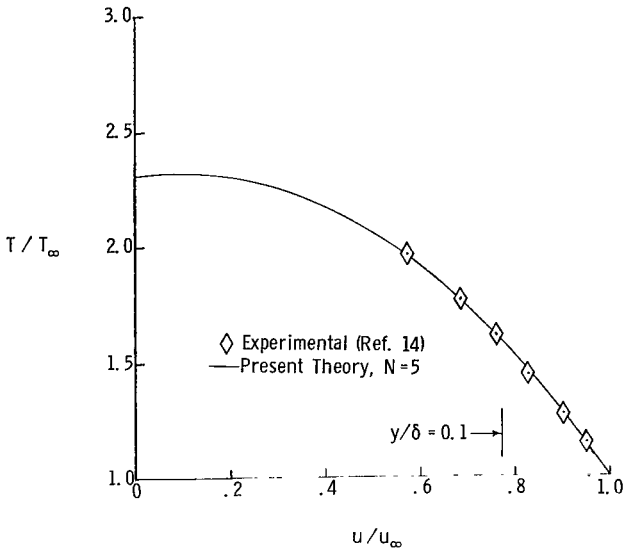

(u) $M_\infty = 2.98$; $T_W/T_\infty = 2.308$.

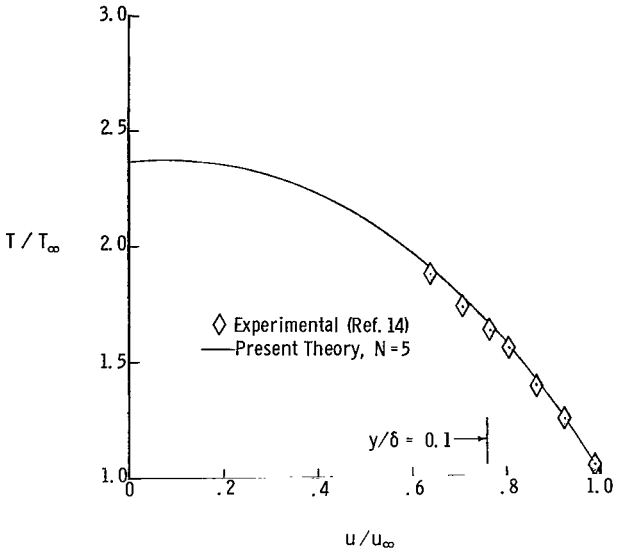

(v) $M_\infty = 2.98$; $T_W/T_\infty = 2.370$.

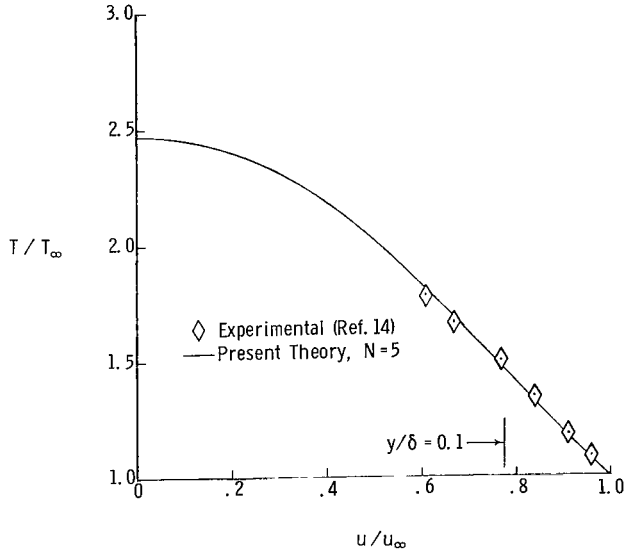

(w) $M_\infty = 2.98$; $T_W/T_\infty = 2.470$.

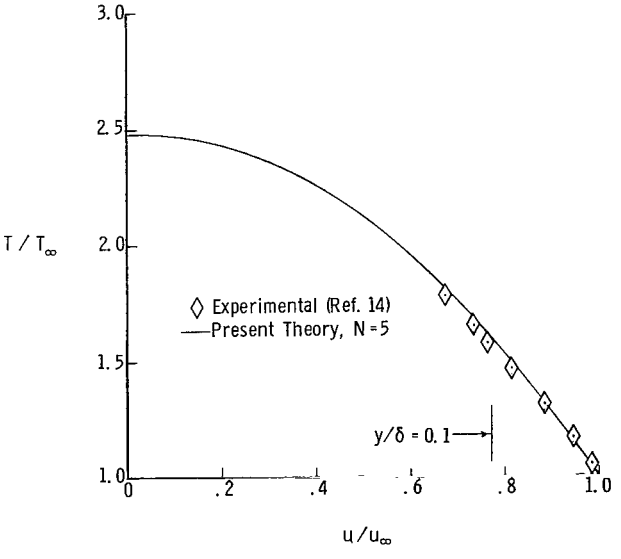

(x) $M_\infty = 2.98$; $T_W/T_\infty = 2.478$.

Figure 9.- Continued.

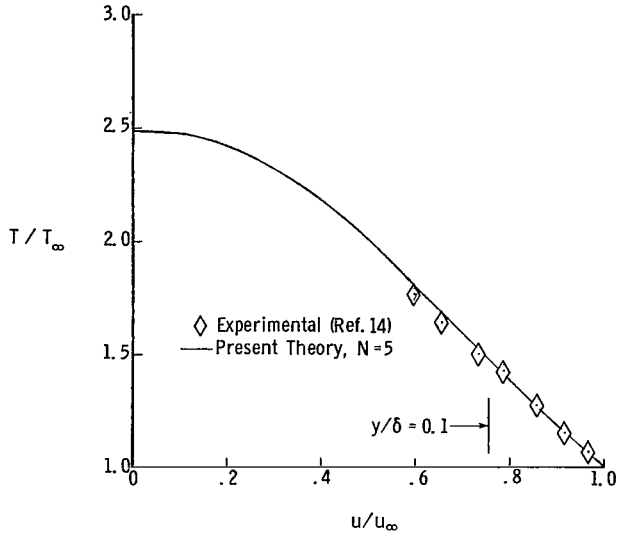

(y) $M_\infty = 2.98$; $T_w/T_\infty = 2.490$.

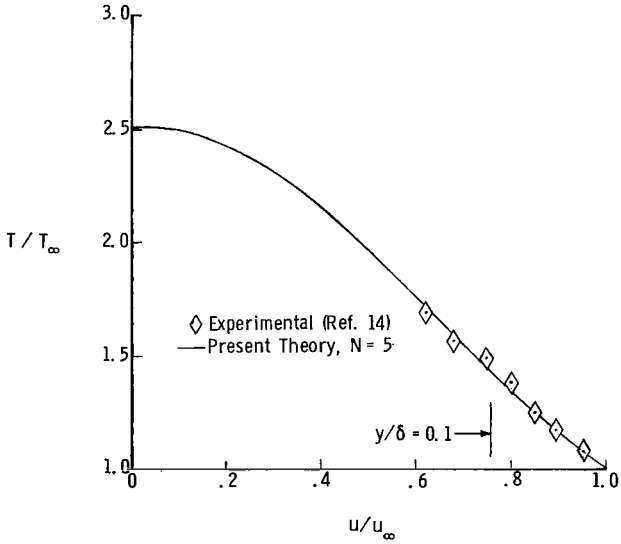

(z) $M_\infty = 2.98$; $T_w/T_\infty = 2.510$.

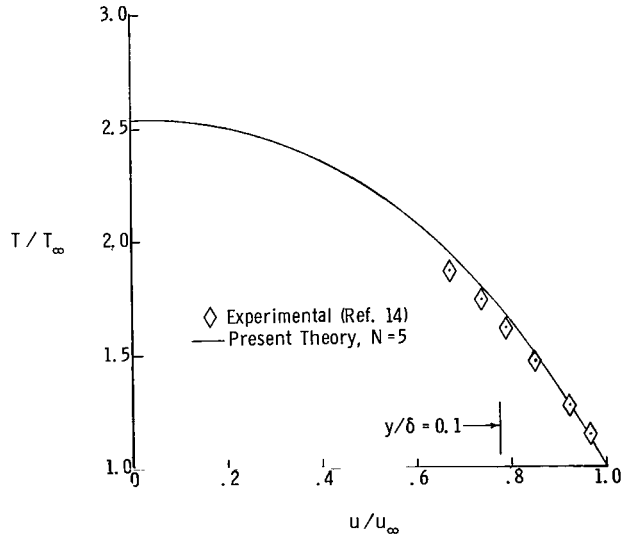

(aa) $M_\infty = 2.98$; $T_w/T_\infty = 2.542$.

Figure 9.- Continued.

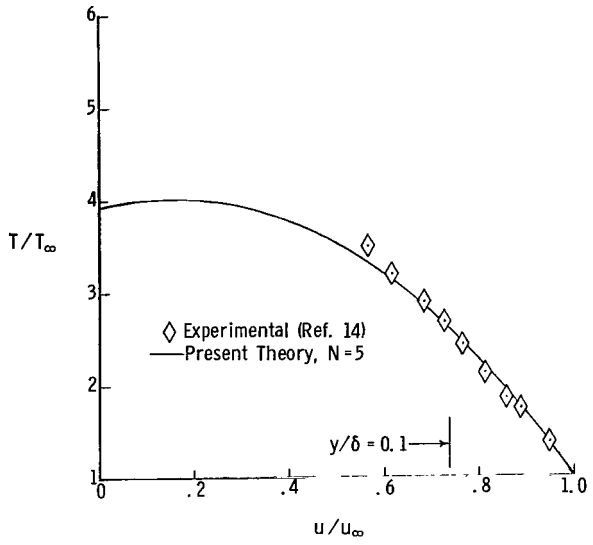

(bb) $M_\infty = 4.88$; $T_W/T_\infty = 3.928$.

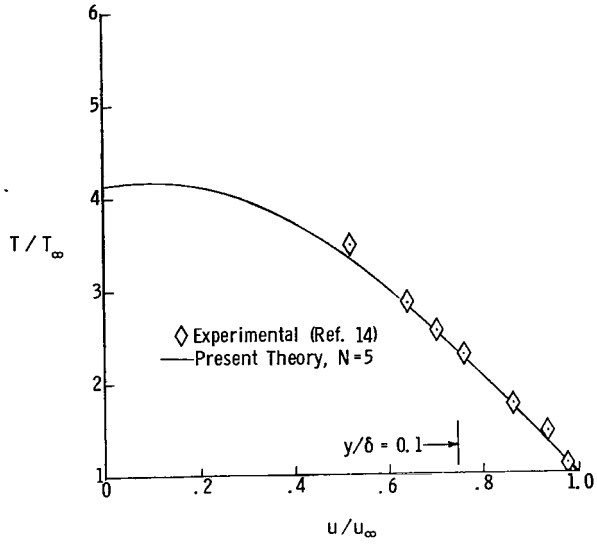

(cc) $M_\infty = 4.88$; $T_W/T_\infty = 4.135$.

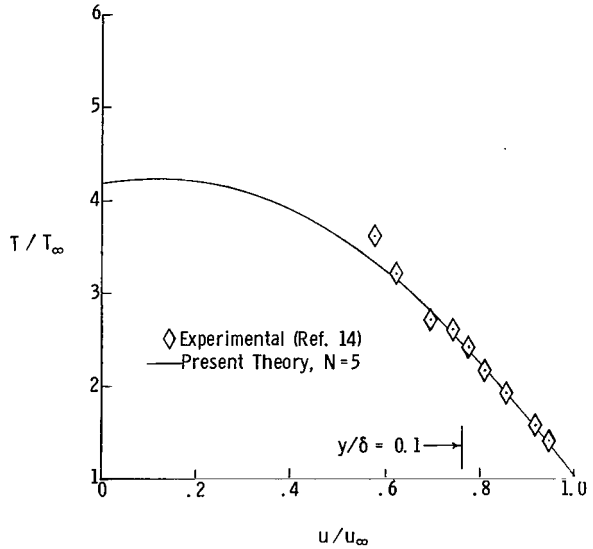

(dd) $M_\infty = 4.88$; $T_W/T_\infty = 4.190$.

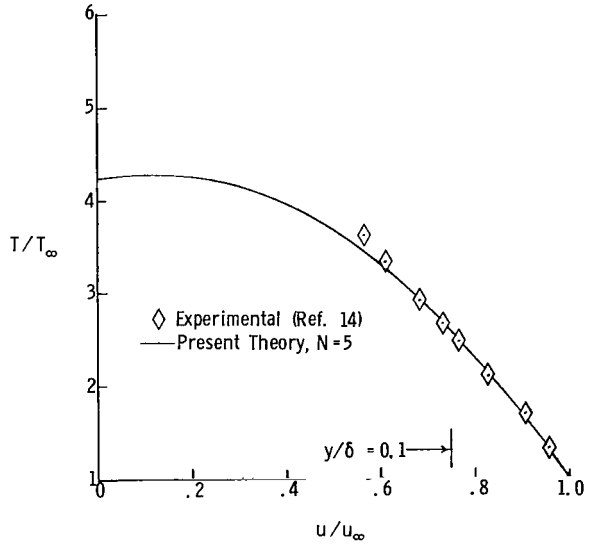

(ee) $M_\infty = 4.88$; $T_W/T_\infty = 4.250$.

Figure 9.- Concluded.

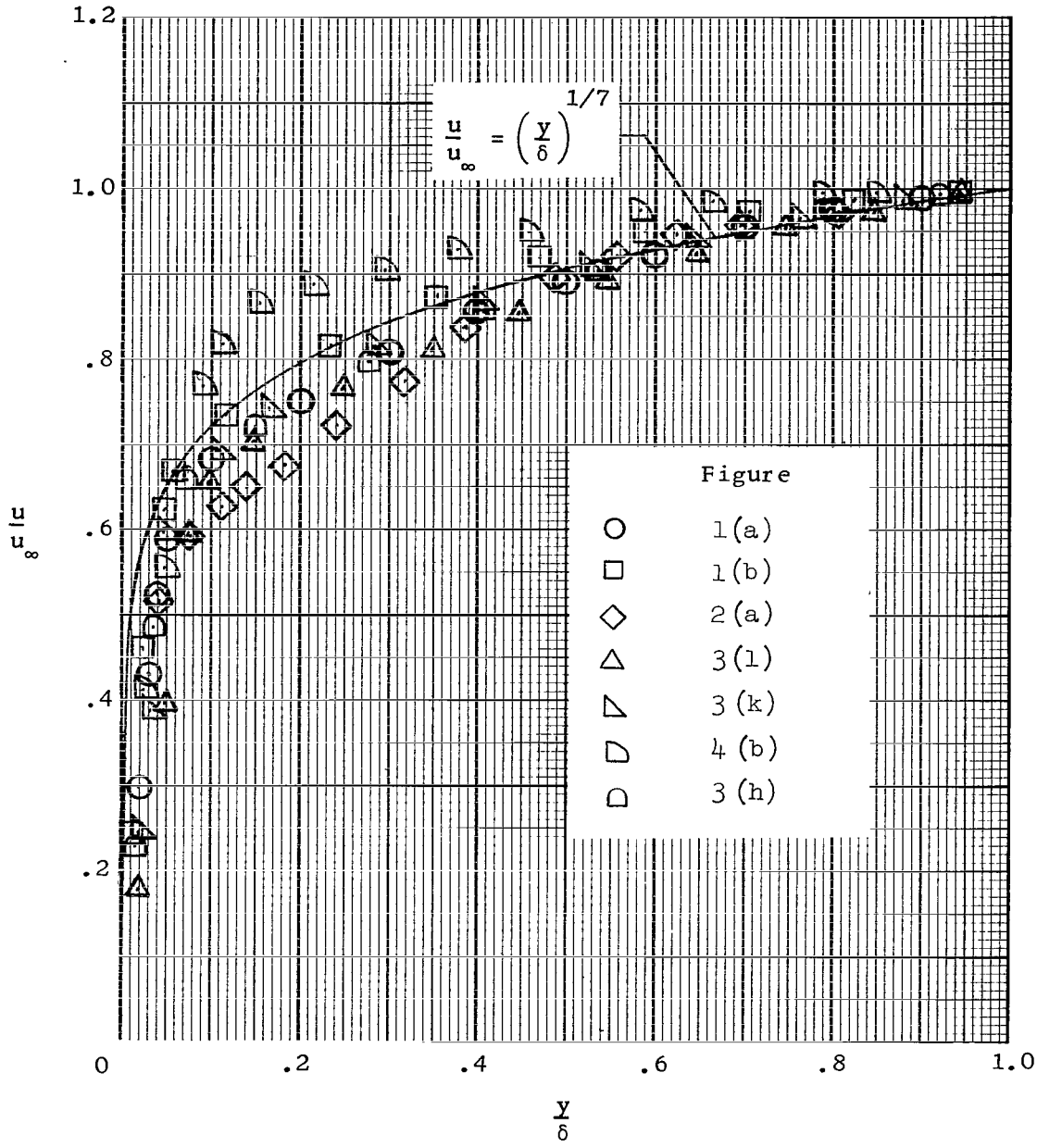

Figure 10.- Experimental boundary-layer velocity profiles corresponding to some of the experimental temperature-velocity profiles in figures 1 to 4.

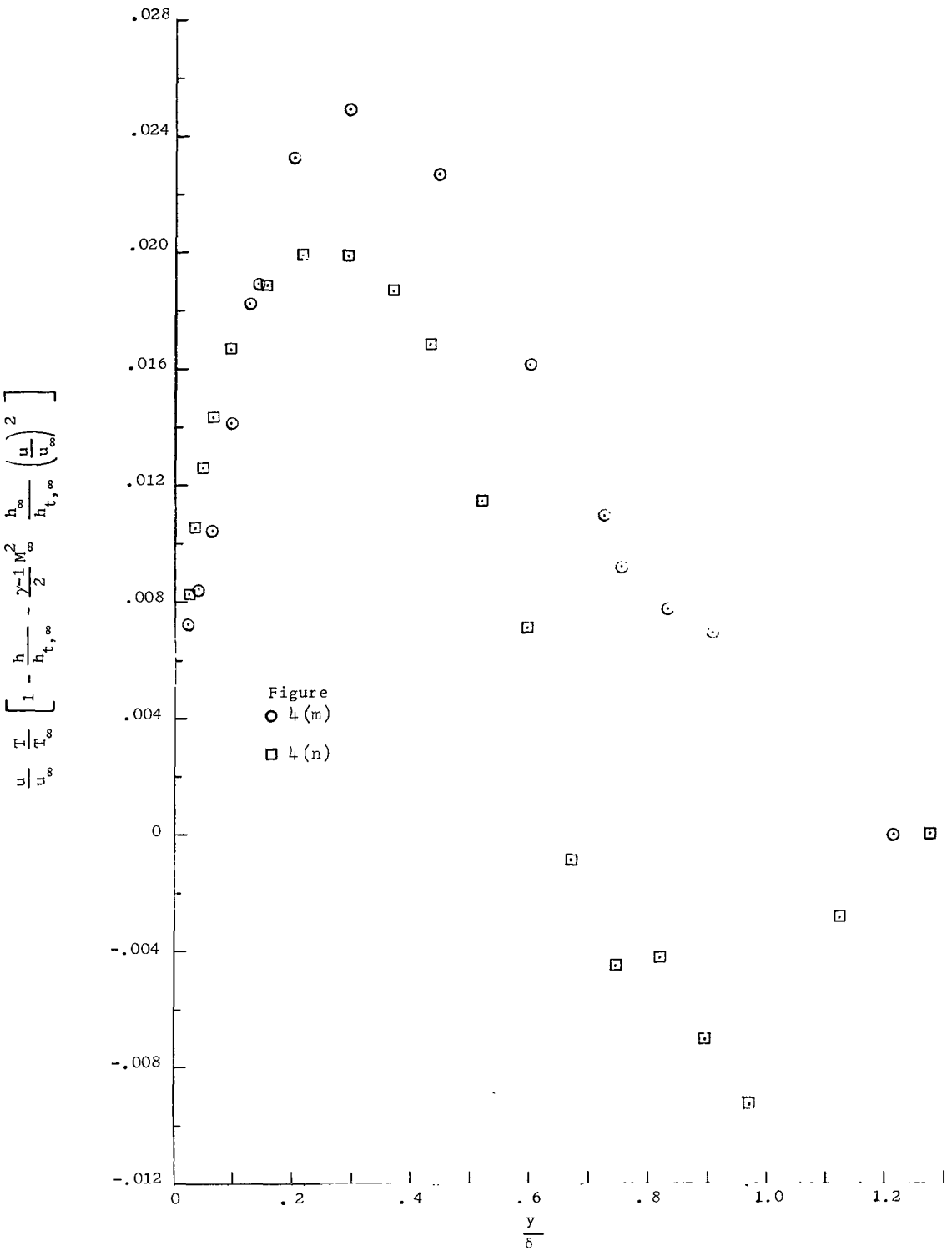

Figure 11.- Energy-deficiency distribution across the boundary layer corresponding to the experimental data of figures 4(m) and 4(n).

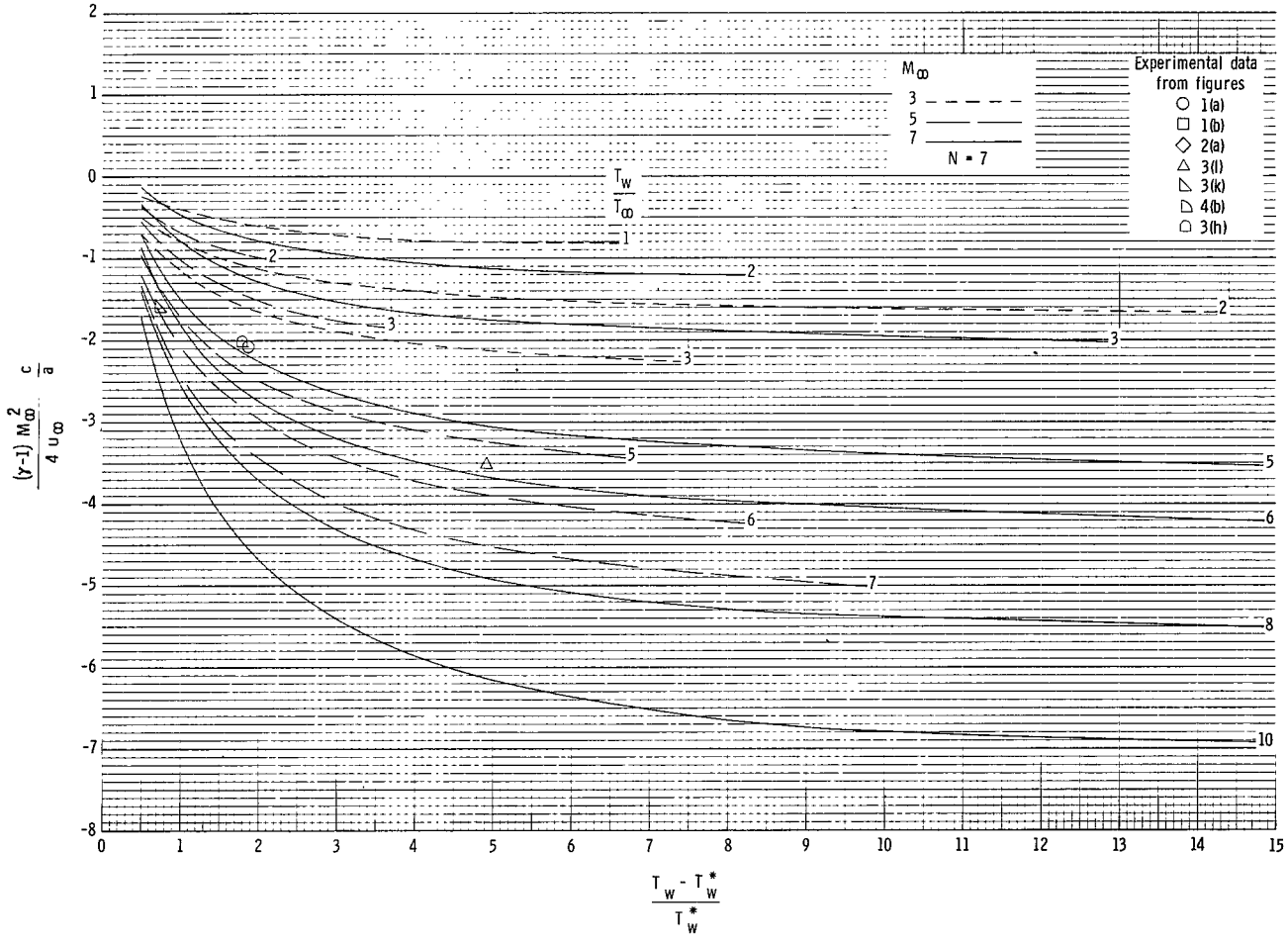

(a) Values of $\frac{T_w - T_w^*}{T_w^*}$ from 0 to 15.

Figure 12.- The energy-deficiency control parameter $\frac{(\gamma - 1)M_\infty^2}{4u_\infty}\frac{c}{a}$ (determined for N = 7) as a function of the deviation of the temperature profile from ideal flat-plate flow, represented by the parameter $\frac{T_w - T_w^*}{T_w^*}$, along with points corresponding to a sampling of the experimental data.

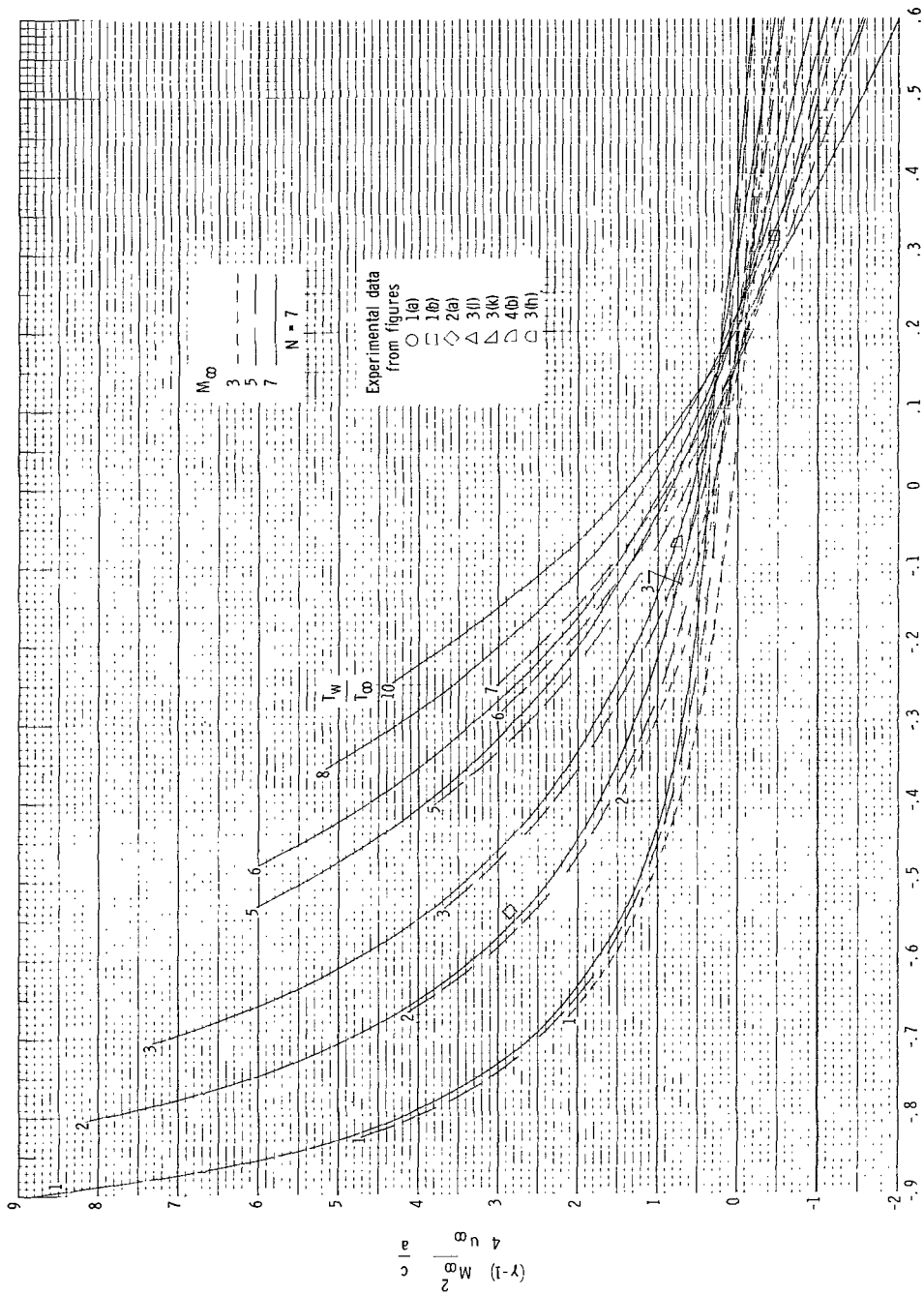

(b) Values of $\frac{T_w - T_w^*}{T_w^*}$ from -0.9 to 0.6.

Figure 12.- Concluded.

NASA-Langley, 1968 —— 12 L-5257

NATIONAL AERONAUTICS AND SPACE ADMINISTRATION
WASHINGTON, D. C. 20546

OFFICIAL BUSINESS

FIRST CLASS MAIL

POSTAGE AND FEES PAID
NATIONAL AERONAUTICS AND
SPACE ADMINISTRATION

POSTMASTER: If Undeliverable (Section 158 Postal Manual) Do Not Return

"The aeronautical and space activities of the United States shall be conducted so as to contribute . . . to the expansion of human knowledge of phenomena in the atmosphere and space. The Administration shall provide for the widest practicable and appropriate dissemination of information concerning its activities and the results thereof."

— NATIONAL AERONAUTICS AND SPACE ACT OF 1958

NASA SCIENTIFIC AND TECHNICAL PUBLICATIONS

TECHNICAL REPORTS: Scientific and technical information considered important, complete, and a lasting contribution to existing knowledge.

TECHNICAL NOTES: Information less broad in scope but nevertheless of importance as a contribution to existing knowledge.

TECHNICAL MEMORANDUMS: Information receiving limited distribution because of preliminary data, security classification, or other reasons.

CONTRACTOR REPORTS: Scientific and technical information generated under a NASA contract or grant and considered an important contribution to existing knowledge.

TECHNICAL TRANSLATIONS: Information published in a foreign language considered to merit NASA distribution in English.

SPECIAL PUBLICATIONS: Information derived from or of value to NASA activities. Publications include conference proceedings, monographs, data compilations, handbooks, sourcebooks, and special bibliographies.

TECHNOLOGY UTILIZATION PUBLICATIONS: Information on technology used by NASA that may be of particular interest in commercial and other non-aerospace applications. Publications include Tech Briefs, Technology Utilization Reports and Notes, and Technology Surveys.

Details on the availability of these publications may be obtained from:

SCIENTIFIC AND TECHNICAL INFORMATION DIVISION

NATIONAL AERONAUTICS AND SPACE ADMINISTRATION

Washington, D.C. 20546